

https://dspace.org/

A fresh look at the physicochemical evolution of the lithospheric mantle beneath the Dharwar craton India

J Pattnaik; S Aulbach; S Ghosh; Robert Bolhar; et al

https://hdl.handle.net/10539/47125
WOS

Downloaded from a DSpace repository. https://dspace.org/

Mineralogy and Petrology (2025) 119:715–741
https://doi.org/10.1007/s00710-025-00943-z

RESEARCH

A fresh look at the physicochemical evolution of the lithospheric mantle beneath the Dharwar craton (India)

Jiten Pattnaik[1,2,3] · Sonja Aulbach[4] · Sujoy Ghosh[1] · E. V. S. S. K. Babu[5] · Fanus Viljoen[2] · Robert Bolhar[6]

Received: 9 December 2024 / Accepted: 11 June 2025 / Published online: 9 July 2025
© The Author(s) 2025

Abstract

The physicochemical evolution of cratonic lithosphere reflects the impacts of tectonomagmatic processes over its lifetime that may be deciphered using kimberlite-borne xenoliths and xenocrysts, but remain poorly constrained for the Indian Dharwar craton, owing to the dearth of fresh mantle material. This study examines detailed petrography and geochemical composition of six eclogite xenoliths, and additional eclogitic and peridotitic garnet separates, from the Wajrakarur kimberlites in the Eastern Dharwar Craton (EDC). Clinopyroxene in eclogite xenoliths is too altered to permit contamination-free sampling during laser ablation for trace element analysis. We overcome this limitation by exploiting relationships of clinopyroxene-garnet distribution coefficients with garnet Ca#, clinopyroxene jadeite content, and temperature. This allows a more accurate delineation of their petrogenesis from reconstructed bulk rocks and indicates their origin from variably plagioclase-rich oceanic crustal protoliths, with weak subsequent metasomatic overprint. In contrast, estimates of Fe^{3+} in garnet from peridotite xenoliths indicate an oxygen fugacity shift towards more oxidized conditions beneath the EDC linked to enrichment in melt-mobile elements (Ti, Zr) in the barren or weakly diamondiferous P1 and P3 kimberlites. The most depleted and reduced sample [$\Delta \log fO_2$ (FMQ) of -4.3; where FMQ corresponds to the fayalite-quartz-magnetite buffer] derives from diamondiferous kimberlite P7, suggesting oxidative melt metasomatism as a key control on the regional diamond inventory, although more data are needed. EDC eclogites and peridotites have estimated P-wave velocities of 8.46–8.63 km/s and 8.21–8.22 km/s, respectively, which are lower than present-day observed bulk P-wave velocities, and may point to lithological or thermal changes since Mesoproterozoic entrainment.

Keywords Grospydite · Kyanite-bearing eclogites · Dharwar craton · Accessory minerals · Metasomatic processes · Seismic velocities · Mass-density characteristics

Editorial handling: D. G. Pearson

✉ Jiten Pattnaik
28jiten@gmail.com

1 Department of Geology and Geophysics, Indian Institute of Technology Kharagpur, Kharagpur, India

2 Department of Geology, University of Johannesburg, Auckland Park, Kingsway Campus, Johannesburg, South Africa

3 Department of Earth and Environmental Sciences, Ben Gurion University of the Negev, David Ben Gurion Blvd, Be'er Sheva 8410501, Israel

4 Goethe-Universität Frankfurt, Institut für Geowissenschaften, Altenhöferallee 1, 60438 Frankfurt, Germany

5 CSIR-National Geophysical Research Institute, Uppal Road, Hyderabad, India

6 School of Geosciences, University of the Witwatersrand, Johannesburg 2001, South Africa

Introduction

Eclogite and pyroxenite are significant minor lithologies in the cratonic lithospheric mantle dominated by peridotite, and they represent ubiquitous constituents of mantle fragments (xenoliths) that are brought up by kimberlites emplaced in the ancient cores of continental lithosphere (Schulze 1989). Eclogites preserve characteristic features of their low-pressure protoliths in their trace element patterns (e.g., Sr and Eu anomalies) and stable isotope compositions (e.g., O, Mg), all of which point to an oceanic crustal origin (Jacob 2004; Aulbach and Smart 2023). The mineralogy (both primary and secondary), chemical composition and redox conditions of xenolithic eclogite may thus help us understand their petrogenesis, monitor the changes that occurred in ancient oceanic crust during subduction and through time, and estimate their contribution to present-day geophysical

signals of the continents (Garber et al. 2018; Aulbach and Smart 2023). Indeed, Garber et al. (2018) demonstrated that mantle eclogite (although subordinate in volume) can play a significant role in determining the electrical conductivity, gravity, and mass density of the lithospheric mantle.

Some eclogite xenoliths contain quartz/coesite or diamond, and many are characterized by kyanite and/or corundum with Ca-rich garnets and jadeite-rich clinopyroxenes, which are known as kyanite/corundum eclogites and grospydites (Smyth et al. 1984; Jacob et al. 2003; Shu et al. 2016; Aulbach et al. 2016; Pattnaik et al. 2025) these are thought to represent relatively pristine eclogite samples (Lappin and Dawson 1975; Sommer et al. 2017). Other accessory minerals, such as plagioclase, mica, and amphibole, along with less common phases like Ba-feldspar (celsian), barite, calcite, apatite, zircon, allanite, among others, are commonly found along cracks and grain boundaries and occasionally as texturally equilibrated matrix minerals. They are often attributed to mantle metasomatism and can provide insights into the late-stage evolution of eclogite, either during its residence in the mantle or upon entrainment in the host kimberlite (Lappin 1978; Carswell et al. 1981; Macgregor and Manton 1986; Caporuscio and Smyth 1987; McCormick et al. 1994; Pyle and Haggerty 1994; Harley and Carswell 1995; Heaman et al. 2002; Ishikawa et al. 2008; Misra et al. 2008; Dawson and Harley 2009; Shchukina et al. 2018; Mikhailenko et al. 2021, 2024; Radu et al. 2022).

As is true for many of the better-studied cratons (e.g. Kaapvaal, Siberian, Slave), eclogite xenoliths have been reported in Mesoproterozoic kimberlite pipes within the Eastern Dharwar Craton (EDC). Most studies focused on their oceanic crustal origin, subsequent mantle metasomatism, and depth distribution within the Dharwar cratonic lithosphere (Ganguly and Bhattacharya 1987; Nehru and Reddy 1989; Patel et al. 2006, 2009; Babu et al. 2008; Dongre et al. 2015; Chatterjee et al. 2023). Combining the $Fe^{3+}/\Sigma Fe$ ratios in garnets from eclogite and peridotite xenoliths with mineral major and trace element concentrations, Shaikh et al. (2023) offer a perspective specifically on the oxygen fugacity (fO_2) of the lithospheric mantle beneath the EDC, but also emphasize the paucity of suitable material for detailed geochemical study. This is because the preservation of mantle material from Dharwar kimberlites is notably poor, and widespread alteration impedes the precise characterization of the physicochemical state and evolution of the regional cratonic lithosphere, which remains severely understudied as a consequence. The characterization of any additional material will therefore not only boost our confidence in the statistical significance of existing data forming the basis of current models of the stratigraphy and evolution of the Dharwar craton, but also has the potential to yield significant new insights.

In this contribution, we provide the detailed petrography (both primary and secondary phases) and major and trace-element compositions of rock-forming and accessory minerals in six new bimineralic and kyanite-bearing eclogites from various kimberlite pipes located within the EDC. We further provide estimates of their seismic velocities and mass densities using geochemical data in this and published studies, which can be contrasted with geophysical models of the present-day EDC lithosphere that depict a severely thinned cratonic root (Dongre et al. 2017 and references therein). Finally, we present Mössbauer spectroscopy-based fO_2 estimates for garnet mineral separates from four peridotite xenoliths and one eclogite xenolith, adding further constraints on the effect of mantle metasomatism on this intensive variable (Yaxley et al. 2012; Hanger et al. 2015; Yaxley et al. 2017; Woodland et al. 2021), which in-part dictates the stability of diamond in the cratonic mantle (e.g., Stagno et al. 2013, 2015).

Building on prior work that has outlined the main petrogenetic features of eclogite and peridotite xenoliths from the EDC, the aims of the present study are: (1) To better document the secondary phases, including rare minerals such as celsian and the rock grospydite, formed by post-peak metamorphic reactions between the eclogite and host kimberlite or metasomatic melts in-situ in the mantle, providing insights into the late-stage evolution of these xenoliths; (2) to evaluate the effect of metasomatism on the oxygen fugacity profile beneath the EDC and its diamond endowment; and (3) to discuss the variations in seismic velocities and mass densities along the lithospheric depths, with implications for the stability and ultimate demise of the originally thick and diamondiferous Dharwar cratonic root.

Geological setting and previous work

Overview

The Archean Dharwar craton in southern India consists primarily of greenstone belts overlying a basement of tonalite-trondhjemite-granodiorite (TTG), known as the Peninsular Gneissic Complex (Naqvi and Rogers 1987). These gneisses have been intruded by multiple generations of Paleoproterozoic granites, among which the Closepet granite, dating back 2.51 billion years (Friend and Nutman 1991), is a prominent feature. The craton is flanked by the Proterozoic Eastern Ghats mobile belt to the east and the Archean Bastar craton to the northeast, while its northwestern edge is capped by Cretaceous-Paleogene lava flows of the Deccan Traps (Ramakrishnan and Vaidyanathan 2010) (Fig. 1). In the eastern region, the granite-greenstone terrane is overlain

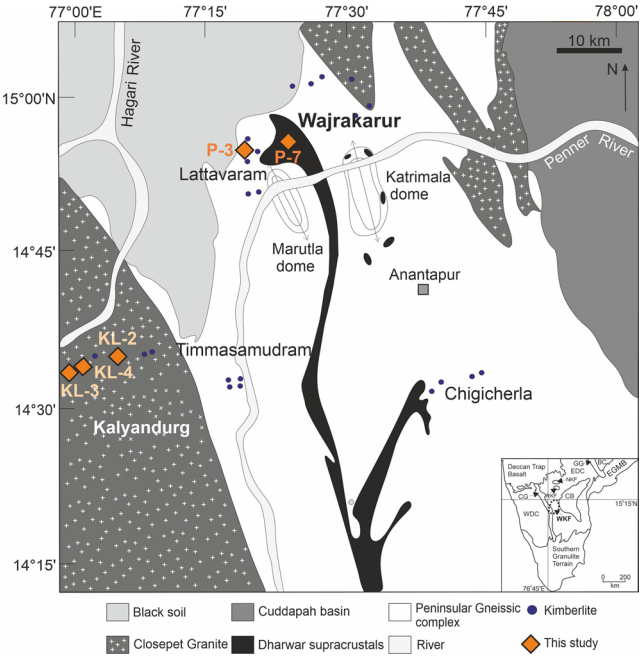


Fig. 1 Geological map of the Wajrakarur kimberlite field (WKF) depicting different clusters of kimberlite pipes emplaced in the Eastern Dharwar craton (Nayak and Kundari 1999). Diamonds indicate kimberlites with eclogite and peridotite xenoliths investigated in this study, and circles indicate kimberlite pipes from other clusters. See inset for location of the WKF in southern India. GG- Godavari graben, BC- Bundelkhand craton, EDC- Eastern Dharwar craton, WDC- Wajrakarur kimberlite field, NKF- Narayanpet kimberlite field, RKF- Raichur kimberlite field, EGMB- Eastern Ghat mobile belt, CB- Chattisgarh basin

unconformably by Mesoproterozoic to Neoproterozoic sedimentary basins, including the Cuddapah basin.

The Dharwar craton is divided into two distinct blocks: The EDC and the Western Dharwar Craton (WDC), which are separated by the Chitradurga Boundary Fault, a conspicuous shear zone (Chadwick et al. 2000; Ramakrishnan and Vaidyanadhan 2010). The EDC and WDC are separated by the Closepet granite, which is about 50 km from the Chitradurga schist belt (Naqvi and Rogers 1987). These blocks differ significantly in crustal lithology and metamorphic grade. The EDC is characterized by north-south trending belts of Neoarchean tonalitic to granodioritic gneisses, interspersed with narrow greenstone belts dating back to ~2.7 billion years (Chadwick et al. 2000; Jayananda et al. 2000; Bidyananda et al. 2003; Ramakrishnan and Vaidyanathan 2010). In contrast, the WDC is dominated by an older gneissic granitoid complex, exhibiting multiphase metamorphism of TTGs ranging from 3.4 to 3.0 billion years (Chadwick et al. 2000; Jayananda et al. 2000; Bidyananda et al. 2003; Ramakrishnan and Vaidyanadhan 2010). The kimberlites-lamproites within the Dharwar craton are primarily concentrated in the EDC and are distributed across three main fields: The Wajrakarur kimberlite (-Lamproite) field (WKF) in the southern part, the Narayanpet kimberlite field (NKF) in the northern part, and the Raichur kimberlite field (RKF) situated between them (Fig. 1). Most pipes in the WKF are known to have low diamond grades (Ravi et al. 2013), and diamonds have not been found in the NKF and RKF (Satyanarayana 2002). Ar-Ar phlogopite dating on kimberlite and U-Pb isotopic systems on phlogopite and perovskite grains, document that they were emplaced during the Mesoproterozoic era, ~1.1 billion years ago. (Gopalan and Kumar 2008; Osborne et al. 2011; Chalapathi Rao et al. 2013). In contrast, lamproites were emplaced earlier, between ~1.23 and 1.5 Ga, predating the kimberlites (Chalapathi Rao et al. 1996, 2013; Kumar et al. 2007a, b; Osborne et al. 2011).

Wajrakarur kimberlite field (WKF)

The WKF, situated in Anantapur district (Andhra Pradesh) in India, covers an area approximately 80 km by 70 km and comprises 48 intrusions categorized into four main clusters: Wajrakarur–Lattavaram (16 intrusions, P1–P16), Chigicherla (5 intrusions, CC1–CC5), Kalyandurg (7 intrusions, KL1–KL7), and Timmasamudram (6 intrusions, TK1–TK6) (Fig. 1) (Smith et al. 2013). Most of these intrusions are kimberlites, although some are lamproites or orangeites, with one exception being the Khaderpet intrusion, which is an ultramafic lamprophyre (Smith et al. 2013).

The kimberlites of the WKF intrude into the granites and gneisses of the EDC (Fig. 1). Detailed descriptions of the constituent pipes within the WKF are provided by Neelakantam (2001). These pipes have a dyke-shaped morphology and can appear circular or pod-like on the surface. The largest of these is the P10 pipe, which is pod-shaped and measures about 1200 m by 1000 m. The P2 pipe, in contrast, is elongated. The KL2 pipe (100 m × 80 m) intrudes the 2.6–2.5 billion years old Closepet Granite. Both the KL2 and P10 pipes have been found to contain diamonds (Neelakantam 2001). A notable feature of the WKF is the – albeit rare – preservation of mantle xenoliths, predominantly peridotite and eclogite. In the Wajrakarur–Lattavaram cluster, pipes P1, P3, P4, and P6 are known to contain mantle xenoliths. The smallest pipe in the region, P3, hosts a diverse array of ultramafic mantle xenoliths (Nehru and Reddy 1989). The KL2 pipe within the Kalyandurg cluster is noteworthy because eclogites comprise ~95% of the xenolith population. In addition, pipes 1–6 include crustal xenoliths and megacrysts of different minerals (Nehru and Reddy 1989). Eclogite xenoliths selected for this study were primarily sourced from Pipe 3, KL2, KL3, and KL4 of the Wajrakarur–Lattavaram and Kalyandurg clusters of the WKF.

Eclogite xenoliths from the WKF have been studied in previous works, focused primarily on understanding the

origin and pressure-temperature state of Dharwar eclogites through major element mineral geochemistry (Ganguly and Bhattacharya 1987; Nehru and Reddy 1989; Patel et al. 2006, 2009; Dongre et al. 2015; Chatterjee et al. 2023; Shaikh et al. 2023). Ganguly and Bhattacharya (1987) and Nehru and Reddy (1989) investigated eclogite xenoliths from the P3 kimberlite pipe, determining that these xenoliths equilibrated at temperatures and pressures of 805 to 1280 °C and 2.4 to 5.4 GPa, respectively. These conditions are indicative of depths ranging from 75 to 174 km, establishing the minimum lithosphere thickness at the time of kimberlite emplacement (Ganguly and Bhattacharya 1987). Major element investigations of eclogitic minerals were conducted by Patel et al. (2006) and Patel et al. (2009), who suggested that the xenoliths were likely formed as magmatic cumulates. Conversely, Dongre et al. (2015) argued that the eclogite xenoliths originated from a crustal gabbroic cumulate material supporting a subduction origin based on mineral chemical studies and oxygen isotope evidence. Chatterjee et al. (2023) reported a rare eclogite xenolith from the Kalyandurg kimberlite containing ultra-high-pressure minerals coesite and majoritic garnet, suggesting it originated > 660 km deep, ascended via a pre-Mesoproterozoic mantle plume, and was entrained in Mesoproterozoic kimberlite (~ 1.1 Ga). Shaikh et al. (2023) estimated $Fe^{3+}/\Sigma Fe$ ratios by electron microprobe-based flank method in garnets from eclogite and peridotitic xenoliths revealing diverse $\Delta \log fO_2$ conditions suggestive of oxidative mantle metasomatism affecting diamond potential in the Dharwar craton.

Present-day state and structure based on geophysical studies

While xenolith studies testify to the presence of a diamondiferous and, therefore, thick cratonic root at the time of emplacement of the Wajrakarur kimberlites ca. 1.1 billion years ago and up until intrusion of late Cretaceous orangeites (Griffin et al. 2009; Dongre et al. 2017), the modern-day lithosphere appears to be much thinner. Geophysical studies, including heat flow, magnetotelluric, and seismic analyses, indicate that the Indian cratonic lithosphere is thinned, likely due to Gondwana's breakup and the Indian plate's northward drift during the Cretaceous (Pandey and Agarwal 1999; Kumar et al. 2007a, b). Interactions with mantle plumes, such as the Marion and Reunion hotspots, are thought to have eroded the lithospheric root, facilitating rapid plate movement (Griffin et al. 2009; Veeraswamy and Raval 2005).

Samples and analytical methods

Samples

Six fresh eclogite xenoliths and garnet mineral separates from four different kimberlite pipes of the Wajrakarur-Lattavaram (P3) and Kalyandurg (KL2, KL3, and KL4) clusters from the WKF were investigated. The eclogite xenoliths are dominantly composed of garnets and clinopyroxenes along with other phases, which include kyanite, celsian, and rutile [Table S1 in the electronic supplementary material (ESM) 1)]. These eclogites are mainly classified as kyanite-bearing and bimineralic (kyanite-free) eclogites (Patel et al. 2006, 2009; Dongre et al. 2015). Bimineralic eclogites comprise 50% (3 out of 6) of the total xenoliths examined, while the kyanite-bearing eclogites account for the remainder. In addition to the eclogites, four garnet mineral separates from peridotites and one garnet separate from eclogite were also investigated, with a primary emphasis on elucidating the oxygen fugacity conditions beneath the Dharwar craton and test links to geochemical indices of mantle metasomatism.

Mineral liberation analyzer

Using an FEI Quanta 600 FEG Mineral Liberation Analyzer (MLA) with two Bruker Xflash X-ray detectors, automated mineralogical examinations of eclogite xenolith thin sections were carried out. The purpose of this procedure was to investigate the distribution and associations between the rock-forming and accessory mineral phases. The degree of mineralogical association of the various minerals with each other were determined. Three standards (Cu, quartz, and Au) were used to calibrate the backscatter electron (BSE) grey level in order to assure accuracy. In addition, the X-ray detectors were calibrated automatically using the Cu standard. Operating parameters included an electron accelerating voltage of 25 keV, a working distance of 13 mm, and a specimen current of 10 nA. The measurements were carried out in GXMAP mode, chosen for its meticulous mapping capability, despite being slower due to X-ray spot analyses being collected on a specified XY grid with a point spacing of 23 µm. Minerals in the accessory and secondary phases were the main focus of the processing of data from the mineral liberation analyzer. The objective of this analysis was to assess the textural relationship between rock-forming and accessory minerals and relate it to the mineral composition of the samples (Fig. 3a, b).

Electron probe micro-analyzer (EPMA)

Major and minor element compositions of the primary and secondary minerals for six eclogite xenoliths and grain

separates of garnets (peridotitic and eclogitic xenoliths), from KL-2, KL-3, KL-4, P3 and P7 kimberlites in the EDC were measured by EPMA using a Cameca SX-100 wavelength dispersive spectroscopy. Operating conditions included a 15 kV acceleration voltage, 20 nA beam current, and 1 µm beam diameter. The electron gun was fired with a LaB_6 source. The counting times for peak measurements were as follows: 22 s for Na, 10 s for Mg and Al, 8 s for Si, 20 s for K, 16 s for Ca, 14 s for Ti and Cr, and 16 s for Mn and Fe. Background measurements were conducted for 44 s for Na, 20 s each for Mg and Al, 16 s for Si, 40 s for K, 32 s for Ca, 28 s for Ti, 26 s for Cr, and 32 s for Mn and Fe. The following silicate and oxide reference materials were used for calibrating the instrument: jadeite (Na), orthoclase (Si, K), diopside (Ca), periclase (Mg), corundum (Al), hematite (Fe), rhodonite (Mn), rutile (Ti), barite (Ba), and chromite (Cr); analytical results were corrected using the ZAF correction program. Detection limits are as follows: 0.0010 wt% for Na, 0.011 wt% for Mg, 0.016 wt% for Al, 0.0091 wt% for Si, 0.0011 wt% for K, 0.0028 wt% for Ca, 0.0027 wt% for Ti, 0.0036 wt% for Cr, 0.0036 wt% for Mn, 0.0035 wt% for Fe and 0.013 wt% for Ni.

Laser ablation-inductively coupled plasma-mass spectrometry (LA-ICP-MS)

The trace element compositions of minerals (garnet, kyanite, celsian and rutile) from six Dharwar eclogites from four different kimberlite pipes and garnet (peridotitic and eclogitic) separates from KL-2, P3 and P7 kimberlite pipes were determined, employing an Australian Scientific Instruments (ASI) Resolution 193 nm ArF excimer system coupled to a Thermo Scientific Fisher sector-field ICPMS (Element XR). Measurements were performed in low-resolution and electrostatic scanning (E-scan) modes. Data were acquired by single spot analysis (80 µm for garnet and 30 µm for kyanite, celsian and rutile), using a laser repetition rate of 10 Hz and a fluence of 3 Jcm^{-2}. Total signal acquisition time was 40–50 s to allow data processing and preparation for the next analysis, comprising 10 s of pre-ablation gas blank and post-ablation washout, plus 20–30 s of ablation measurements. Laser sampling took place in a SE155 dual-volume ablation cell (Laurin Technic, Canberra, Australia) using a mixed He-Ar atmosphere and a small volume of N_2 to enhance signal stability and sensitivity. The following gas flows were typically applied: He (350 ml/min), Ar (1000 ml/min) and N_2 (5 ml/min), respectively. Synthetic glass NIST 612 (Jochum et al. 2011) served for sensitivity calibration, while a USGS natural glass (BCR 2G) was analyzed as unknown to evaluate accuracy and precision [Table S2 in the ESM1]. The LA-ICPMS system was tuned during line scans using NIST 612 glass for maximum sensitivity for ^{59}Co, ^{115}In and ^{232}Th, while maintaining oxide levels (ThO+/Th) < 0.12%. Prior to each spot analysis surface material was removed using 2 laser pulses. The following masses were measured: ^{7}Li, ^{9}Be, ^{24}Mg, ^{27}Al, ^{29}Si, ^{44}Ca, ^{45}Sc, ^{49}Ti, ^{51}V, ^{52}Cr, ^{55}Mn, ^{59}Co, ^{60}Ni, ^{63}Cu, ^{66}Zn, ^{69}Ga, ^{72}Ge, ^{85}Rb, ^{89}Y, ^{90}Zr, ^{93}Nb, ^{95}Mo, ^{107}Ag, ^{107}Cd, ^{118}Sn, ^{121}sb, ^{133}Cs, ^{137}Ba, ^{139}La, ^{140}Ce, ^{141}Pr, ^{146}Nd, ^{147}Sm, ^{151}Eu, ^{157}Gd, ^{159}Tb, ^{163}Dy, ^{165}Ho, ^{166}Er, ^{169}Tm, ^{174}Yb, ^{175}Lu, ^{178}Hf, ^{181}Ta, ^{182}W, ^{197}Au, ^{208}Pb, ^{232}Th, ^{238}U. All isotopes were measured in triple mode, including pulse counting, analog and Faraday cup, depending on the signal.

For internal calibration, the isotope ^{29}Si (garnet) was used. Typically, two analyses of the primary calibration standard were obtained at the beginning and end of an experiment, and 10–20 analyses of unknowns were followed by analyses of one primary calibration standard and analyses of the reference materials for quality control purposes. Comparison to accepted values (Jochum et al. 2005) indicates that all elements were accurately quantified within 7%, with the exception of Ti, Cu and Ge, which were quantified within 11%.

Data reduction was performed using the iolite extension (http://www.iolite.org. au; accessed 19 April 2025) to the software Igor Pro (http://www.wavemetrics.com; accessed 19 April 2025), specifically the data reduction scheme ("DRS") "X_Trace Elements_IS", proceeding in a series of sequential steps, including data import, selection of integrations, baseline subtraction, drift and down-hole fractionation, calibration, and error propagation (Paton et al. 2010, 2011). For each mineral, 1 to 5 spots were analyzed per grain, using an 80 µm laser spot size for garnet and a 30 µm laser spot size for kyanite, celsian and rutile, targeting the grain cores. Utmost care was taken to perform analyses on only crack-free, fresh and unaltered areas of the minerals.

Methodology for estimation of trace element concentrations in clinopyroxenes coexisting with garnet in xenolithic eclogites and pyroxenites

The incorporation of many trace elements into eclogitic garnet and clinopyroxene is markedly temperature- and composition-dependent (O'Reilly and Griffin 1995; Harte and Kirkley 1997). As a consequence, only reconstructed bulk rocks provide a robust framework for a complete understanding of the petrogenesis of mantle-derived eclogitic and pyroxenitic samples within and across diverse cratons. To tackle the issues of kimberlitic contamination and alteration in clinopyroxenes, which precludes the acquisition of accurate data by LA ICPMS with spot sizes at least an order of magnitude larger than required by EPMA, we devised a novel approach to estimate their trace element concentrations through the integration of a carefully selected,

isogenous dataset of eclogite and pyroxenite xenoliths, and incorporated additional data for the Dharwar craton from Dongre et al. (2015) (ESM2). This enabled the analysis of the dependence of trace element distribution *D* on key parameters - garnet Ca#, jadeite content in clinopyroxene, and temperature (see Results for details on temperature estimates; also Fig. S5b in the ESM3). The trace element concentration in clinopyroxene was then estimated from that in garnet as a function of the parameter yielding the highest r^2 value (ESM2). We do not report results for elements with consistently low r^2 (<0.20), such as Rb and Nb, due to limited observations and contamination susceptibility. Calculated uncertainties for cpx trace element concentrations were derived from residual analysis (Table S15 a, b in the ESM2).

Mössbauer spectroscopy

Ratios of $Fe^{3+}/\Sigma Fe$ in garnet crystals separated from four peridotite and one eclogite xenoliths (Fig. S6 in the ESM3) were determined using Mössbauer spectroscopy. Fresh, inclusion-free and homogeneous garnet crystals were carefully selected under a stereomicroscope and subsequently powdered with an agate mortar in ethanol. Approximately 10 mg of the powdered sample was loaded into a sample holder, and data collection spanned 72 h. The room-temperature transmission ^{57}Fe Mössbauer spectrum of the powdered samples was recorded utilizing a Mössbauer spectrometer operating in constant acceleration mode, with a 25 mCi ^{57}Co (Rh) source of γ-rays from Ritverc products. Acquisition of Mössbauer data was facilitated by the Wissoft CMCA-550 module within the Multichannel Scaling window. The resulting Mössbauer spectrum was obtained using Lorentzian line shapes and fitted using the WinNormos software for the IGOR Pro package, employing the least-squares method. The final fitting model comprised two doublets: one corresponding to Fe^{2+} and the other to Fe^{3+}.

Hyperfine parameters such as δ (isomer shift), ΔEQ (quadrupole splitting), W (full width at half maximum), and RA (relative spectral area) were determined through the fitting procedures (see Table S11 in the ESM1). Isomer shift values were referenced to a metallic Fe foil sample at room temperature. These parameters allowed for the estimation of the relative amounts of Fe^{2+} and Fe^{3+} in the samples. The $Fe^{3+}/\Sigma Fe$ ratios in the garnet crystals were determined with an error margin of ±0.01, and these values are presented in Table S14 in the ESM1.

Results

Petrography

The bimineralic eclogites are coarse-grained, granular rocks primarily consisting of garnet and clinopyroxene. The size of the hand specimens ranges from 2 to 4 cm. In hand specimens, these samples are dominated by whitish clinopyroxene and greyish garnet affected by alteration. Macroscopically, garnet is subhedral to anhedral in shape, and medium- to coarse-grained (Fig. S1 in the ESM3). Clinopyroxene is anhedral and occurs in the interstices, enclosing the garnet. Fresh and clear portions of grain cores of garnet and clinopyroxene were used for major element and in-situ trace element analyses. The summary of the mineral assemblage of the eclogite xenoliths from different pipes and the details of the mineral separates from different kimberlite pipes are given in Table 1.

In thin section, garnet is faintly pink and mainly 2–8 mm in size. The grains have noticeable fracturing and sometimes these fracture planes may be filled with serpentine, calcite or a Ba-rich sulfate or carbonate (Fig. 2a, b). Clinopyroxene appears dull white to cloudy greenish, with grain sizes ranging from 1 to 8 mm. It exhibits extensive alteration, preserving only a few remnants of fresh grain cores, and features irregular grain boundaries (Fig. S1a in the ESM3). The majority is crisscrossed by carbonate veins and shows extensive alteration, with the degree of alteration exceeding 50% based on visual estimates. A calcite veinlet is identified in one of the eclogite samples (*P*3-10) (Figs. 3c and d and 2a). Rutile occurs in one of the samples (P3-10) as a discrete grain (Fig. 2e, f). Kyanite is present in less than 5 vol% in 3 eclogite xenoliths [Table S1 in the ESM1]. It is anhedral in shape and ranges from 0.5 to 1 mm in size (Fig. 2g). It occurs adjacent to clinopyroxene and is partially replaced/rimmed by celsian (Fig. 2h). Quartz/coesite is also identified in one of the samples (KL3-ECG-13) (Fig. 2i). Celsian (100–300 μm) is anhedral in shape, and typically rims kyanite (Fig. 2j), but also fills fractures in garnet.

Major element compositions

Average major- and trace-element concentrations in garnet, clinopyroxene, kyanite, celsian, rutile and ilmenite, are described below and listed in Tables 2, 3, 4 and 5 and in Tables S12 and S13 in the ESM1. Results of individual analyses of the mineral phases in the eclogite xenoliths and mineral separates of all the samples are reported in Tables S3 to S9 in the ESM1.

Garnet compositions vary significantly: Mg# [molar $Mg/(Mg+Fe_{total})$] ranges from 0.49 to 0.71, Ca# [molar $Ca/(Ca+Mg+Fe_{total}+Mn)$] from 0.25 to 0.55, and Cr# [molar

Table 1 Mineral assemblage as well as estimates of physical properties of eclogite xenoliths in kimberlite pipes of Eastern Dharwar craton

Number	Sample	Xenolith type	Mineral assemblage**	T[a] (°C)	*P*[a] (GPa)	ρ[b] (g/cm^3)	[b]Vp (km/s)	[b]Vs (km/s)
1	KL2-B1	Eclogite	Grt, Cpx, Ky	1098	4.6	3.57	8.63	4.91
2	KL3-L	Eclogite	Grt, Cpx	1026	4.3	3.56	8.56	4.83
3	KL3-ECG-13	Eclogite	Grt, Cpx	898	3.6	3.61	8.57	4.84
4	KL3-S	Eclogite	Grt, Cpx, Ky	1088	4.6	3.57	8.59	4.87
5	KL4-D2-6	Eclogite	Grt, Cpx, Ky	1122	4.8	3.58	8.60	4.86
6	P3-10	Eclogite	Grt, Cpx	726	2.6	3.62	8.46	4.80
7*	KL2	Eclogite	Grt	913	3.7	n.a	n.a	n.a
8*	KL2 G1	Eclogite	Grt	n.a	n.a	n.a	n.a	n.a
9*	KL2 G2	Eclogite	Grt	n.a	n.a	n.a	n.a	n.a
10*	KL2 G3	Eclogite	Grt	n.a	n.a	n.a	n.a	n.a
11*	P3	Peridotite	Grt	1035	4.3	n.a	n.a	n.a
12*	P3P	Peridotite	Grt	1013	4.2	n.a	n.a	n.a
13*	P7	Peridotite	Grt	1226	5.4	n.a	n.a	n.a
14*	P1P2	Peridotite	Grt	1243	5.5	n.a	n.a	n.a

* Mineral separates recovered from the xenoliths

** Cpx – clinopyroxene; Grt – garnet; Ky – kyanite

[a] Temperatures obtained from the Krogh (1988) thermometer for eclogites and Sudholz et al. (2021) thermometer for peridotites were solved iteratively with pressures (P) parameterized from the 40 mW/m^2 conductive geotherm of Hasterok and Chapman (2011). The discrepancies for T are mostly within ± 50 °C (for eclogites) and ± 55 °C (for peridotites), which results in an uncertainty in iteratively calculated pressures at around ± 0.3 GPa. Discrepancies refer to the estimated uncertainties in the thermobarometer formulation

[b] Calculated from the spreadsheet of Abers and Hacker (2016) at the estimated pressures and temperatures using the grt and cpx end members

n.a = not available

Cr/(Cr + Al+)] from 0.0004 to 0.001. Garnet in kyanite-bearing eclogites typically exhibits higher median Mg# (0.56) and Ca# (0.45) compared to that in bimineralic eclogites (0.50 Mg# and 0.32 Ca#). Contents of Na_2O range from 0.04 to 0.11 wt%. Other minor elements include TiO_2 (0.08 to 0.23 wt%) and MnO (0.16 to 0.35 wt%). Garnet compositions vary widely in Mg-Fe-Ca end members (Fig. S2b in the ESM3), typically comprising 26 to 51 mol% pyrope, 19 to 36 mol% almandine, and 21 to 47 mol% grossular ("Group-B" in the classification of Coleman et al. 1965; Fig. S2b in the ESM3). Exceptions are KL2-B1 and KL4 D2-6, which have garnet with up to 91 mol% grossular component that is qualified as grospydite garnet (Sobolev et al. 1977), which are classified as Group-C according to Coleman et al. (1965). All these garnets are Ca-rich, as they plot within the high-Ca field according to the classification scheme of Aulbach and Jacob (2016) (Fig. 4b).

The peridotitic garnet separates from three kimberlite pipes (P1, P3 and P7) are predominantly pyrope-rich. Its compositions in terms of Cr_2O_3 and CaO contents (wt%) indicate distinct source parageneses: Lherzolitic (P1, P3) and harzburgitic (P7; Fig. S2a in the ESM3, Table S14 in the ESM1). Lherzolitic garnet exhibits a lower Mg# (median 0.82), contrasting with the higher Mg# of harzburgitic garnet (0.87). The FeO and CaO contents vary between 5.50 and 8.03 wt% and 3.95 to 4.66 wt%, respectively. The Cr# in lherzolitic garnet is 0.01, markedly lower compared to harzburgitic garnet (0.18). Furthermore, lherzolitic garnet displays higher Al_2O_3 contents ranging from 21.71 to 23.20 wt%, in contrast to harzburgitic garnet (18.59 wt%).

Clinopyroxene exhibits considerable variability in Mg# (0.81 to 0.90), Cr# (0.002 to 0.006), and jadeite content (0.22 to 0.47). In all samples, it falls in the omphacite field of the Morimoto 1989 classification (Fig. S3a in the ESM3). Clinopyroxene from bimineralic eclogites generally shows higher Mg# (median 0.89) compared to that from kyanite-bearing eclogites (median 0.87). Kyanite-bearing eclogites, however, tend to have clinopyroxene with higher jadeite contents (median 0.43) compared to that in bimineralic eclogites (median 0.33). The MgO and Na_2O contents range from 7.26 to 11.59 wt% and 3.22 to 6.71 wt%, respectively, placing the samples within group B eclogites (Taylor and Neal 1989) as shown in Fig. S3b in the ESM3. The contents of CaO range from 12.72 to 19.02 wt%.

Clinopyroxene in bimineralic eclogites have higher Cr_2O_3 contents (median 0.07 wt%) than in kyanite-bearing eclogites (median 0.03 wt%). Similarly, FeO contents range from 1.86 to 3.10 wt%, with a higher median in bimineralic eclogites (2.75 wt%) compared to kyanite-bearing eclogites (2.45 wt%). The contents of K_2O vary from 0.01 to 1.78 wt%, with higher levels found in clinopyroxene from bimineralic eclogites (median 0.06 wt%) compared to that from kyanite-bearing ones (median 0.02 wt%). Contents of TiO_2 range from 0.04 to 0.52 wt%, with bimineralic eclogites containing more (median 0.39 wt%) than kyanite-bearing eclogites (median 0.14 wt%). The Na_2O contents decrease with the decrease in TiO_2 contents in the garnet, roughly at

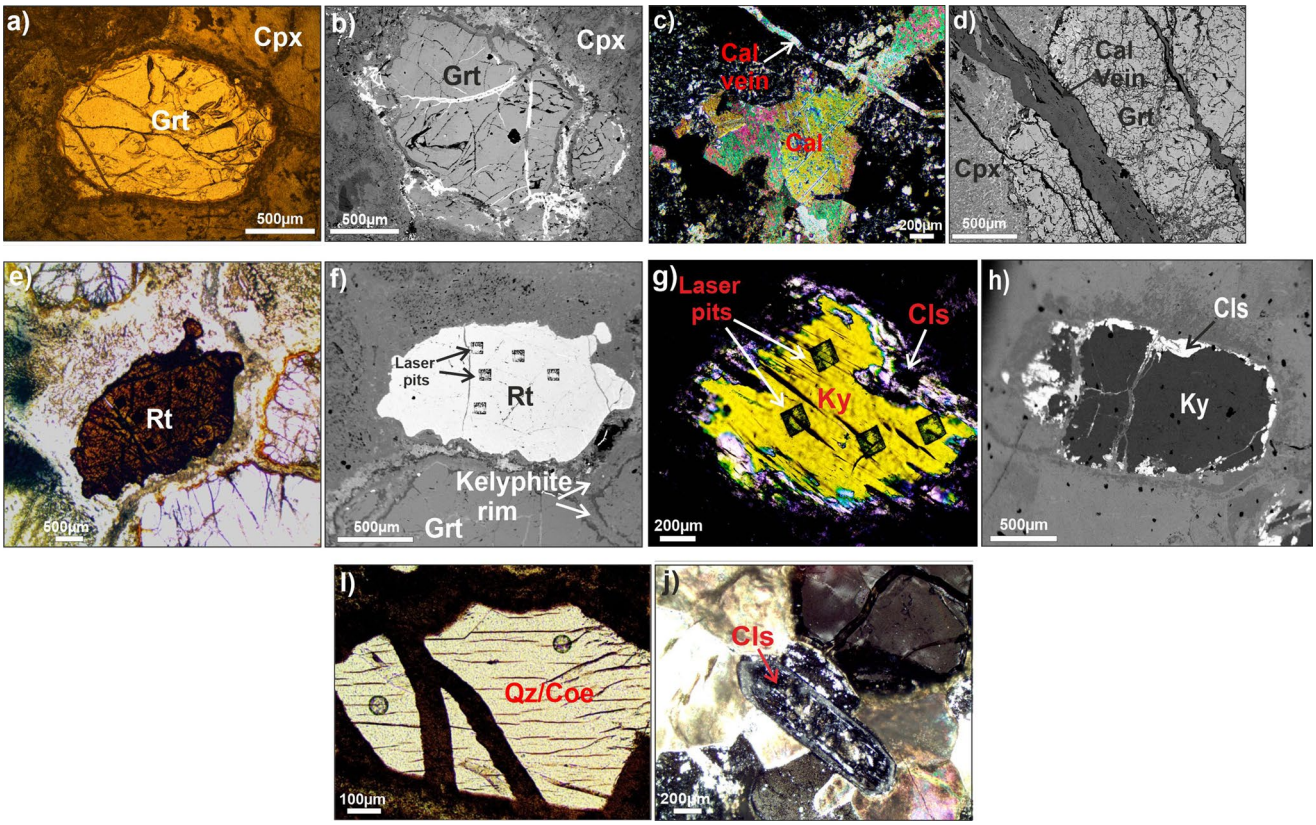


Fig. 2 High-magnification photomicrographs and backscattered electron (BSE) images of mineral grains and assemblages in eclogite xenoliths from the WKF, Eastern Dharwar craton. (**a**) Photomicrograph (plane-polarized transmitted light) of fractured garnet grain set in a matrix of clinopyroxene in sample KL3-S. (**b**) BSE image of a large garnet crystal in sample KL2-B1 displaying a kelyphitic rim. Fractures in garnet are filled with celsian. (**c**) Photomicrograph (cross-polarized transmitted light) of a calcite veinlet in eclogite xenolith P3-10. (**d**) BSE image of a calcite vein crosscutting garnet and clinopyroxene in sample P3-10. (**e**) Photomicrograph (plane-polarized transmitted light) of a rutile grain with irregular grain boundaries in sample P3-10. (**f**) BSE image of a rutile grain occurring in clinopyroxene matrix in sample P3-10. (**g**) Photomicrograph (cross-polarized transmitted light) of a kyanite grain rimmed by celsian in sample KL2-B1. (**h**) BSE image of a kyanite grain rimmed by celsian occurring in clinopyroxene matrix in sample KL2-B1. (**i**) Photomicrograph (cross-polarized transmitted light) of a quartz/coesite grain in sample KL3-ECG-13. (**j**) Photomicrograph (cross-polarized transmitted light) of a celsian feldspar in sample KL3-S. Grt – garnet; Cpx – clinopyroxene; Rt – rutile; Cal – calcite; Ky – kyanite; Cls – celsian; Qz – quartz; Coe – coesite

a slope of unity (Fig. S5a in the ESM3). Additionally, Al_2O_3 contents range from 8.49 to 14.52 wt%, with kyanite-bearing eclogites having a higher median (12.17 wt%) compared to bimineralic eclogites (10.48 wt%). All samples contain clinopyroxene with Na/(Na + Ca) > 0.2, characteristic of true eclogites (Aulbach and Jacob 2016) (Fig. 4a).

Kyanite is present in half of the eclogite samples (3 out of 6) [Table S1 in the ESM1] and shows compositional homogeneity. The SiO_2 and Al_2O_3 contents range from 36.76 to 37.60 wt% and 61.64 to 62.13 wt%, respectively, consistent with findings from kyanite-bearing eclogites documented by Patel et al. (2006). These samples also exhibit minor amounts of Cr_2O_3 (< 0.07 wt%). *Celsian* occurs as a secondary phase in two kyanite-bearing eclogites (KL2-B1 and KL4-D2-6). The BaO content ranges from 38.87 to 39.26 wt%, while Al_2O_3 and FeO content vary from 26 to 27.00 wt% and 0.01 to 0.12 wt%, respectively. The combined $Na_2O + CaO + K_2O$ content is less than 0.60 wt%. In sample P3-10, a *rutile* grain is present as an accessory phase, containing 0.55 wt% Al_2O_3 and 0.57 wt% FeO.

Trace element compositions

Chondrite-normalized rare earth element (REE) concentrations of *garnets* (denoted by subscript N, based on McDonough and Sun 1995) exhibit variations of approximately one order of magnitude. Garnet typically shows depletion in light rare earth elements (LREE), with chondrite normalized La contents (La_N) ranging from 0.03 to 0.73 (see Fig. 5a). Most garnet grains display relatively flat (group I) to slightly enriched (group II) patterns in heavy rare earth elements (HREE), with $(Dy/Yb)_N$ ratios ranging from 0.75 to 1.62. All garnets exhibit varying degrees of europium anomalies, with Eu/Eu* ratios (chondrite-normalized Eu*= Eu/(Sm*Gd)^0.5; chondrite of Sun and McDonough 1989) ranging from 0.1 to 1.4. Concentrations of Ti range from

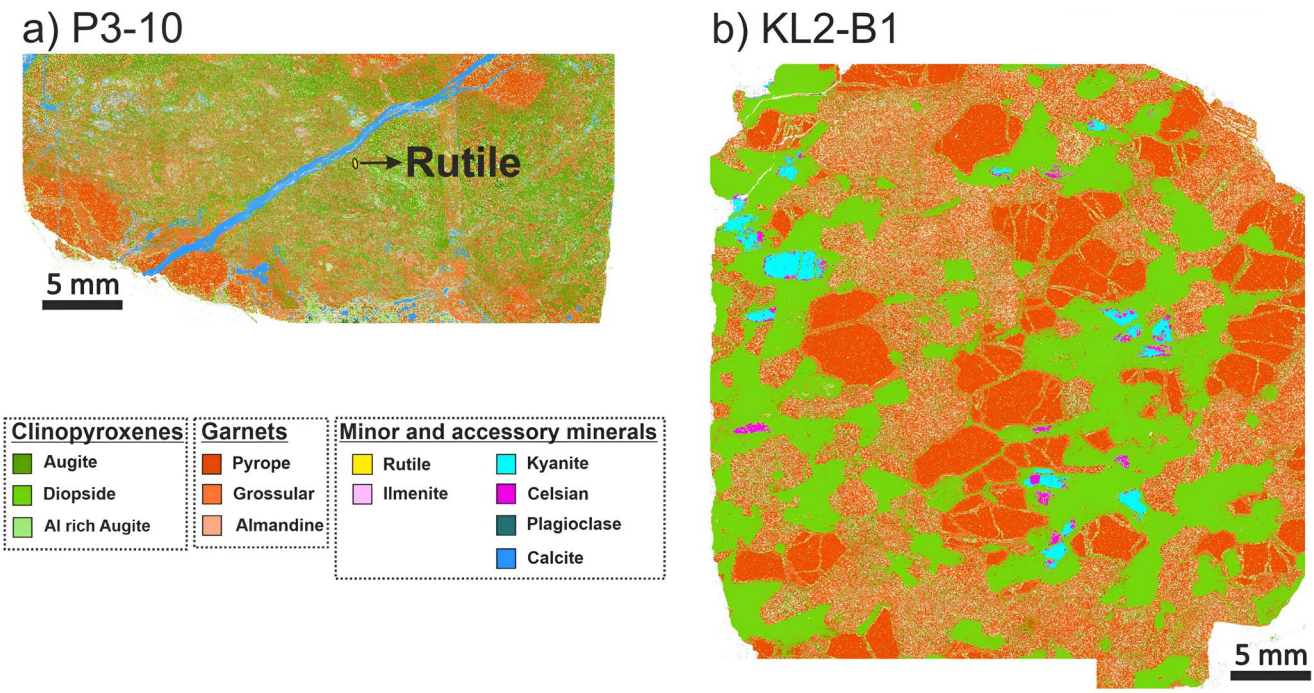


Fig. 3 Mineral liberation analyzer maps obtained from the thin sections of (**a**) bimineralic eclogite (sample P3-10) and (**b**) kyanite eclogite (sample K2-B1). Note calcite vein in the former and shape-preferred orientation of pyroxene in the latter

830 to 6611 ppm, Sr from 0.64 to 6.57 ppm, Y from 4.46 to 67.17 ppm, Zr from 2.77 to 101.13 ppm, and Nb up to 4.45 ppm, broadly aligning with global databases for eclogitic garnet (Jacob 2004). The (Ce_N/Yb_N) ratio varies from 0.005 to 0.65, and total REE concentrations (ΣREE) range from 8.9 to 47 ppm.

Based on their chondrite-normalized REE (REE_N) patterns (McDonough and Sun 1995), the peridotitic garnets from the EDC exhibit distinct characteristics: (1) The lherzolitic garnet grains (P1P2, P3, P3P) exhibit a humped shape with broad peaks in the middle rare earth elements ($MREE_N$); (2) The harzburgitic garnet (P7) displays a sinusoidal pattern, with a peak at Eu (Fig. S4 in the ESM3).

Clinopyroxene exhibits distinctive REE_N patterns, characterized by a steep incline from enriched LREEs (Sm_N/La_N = 0.13 to 0.78) to depleted HREEs (Lu_N/Gd_N = 0.04 to 0.16). These patterns are similar to those reported by Dongre et al. (2015) in group I, with the exception of one sample (P3-10) that is similar to group II. Furthermore, all clinopyroxene grains exhibit significant positive europium anomalies, with Eu/Eu* ratios ranging from 1.16 to 3.13 (Fig. 5b). Kyanite-bearing eclogites tend to exhibit higher Eu/Eu* values than bimineralic eclogites.

Kyanite shows relatively minor concentrations of trace elements compared to other minerals. Titanium and Sr contents range from 317 to 348 ppm and 0.70 to 0.89 ppm, respectively. Ba concentrations in kyanite range from 39 to 47 ppm and Cr concentrations range from 246 to 668 ppm.

The concentrations of trace elements in the *celsian* exhibit a narrow compositional range. Titanium, V, Rb, and Sr contents range from 333 to 341 ppm, 120 to 122 ppm, 16 to 19 ppm, and 594 to 604 ppm, respectively. Additionally, REEs such as La, Eu, and Gd exhibit higher concentrations, ranging from 42 to 47 ppm, 54 to 58 ppm, and 5 to 6 ppm, respectively.

To the extent that this can still be ascertained in markedly altered samples, the Dharwar eclogites are characterized by garnet-in-clinopyroxene-matrix to interlocking texture, whereby the kyanite-bearing samples feature a foliation and mineral banding. Given the degree of alteration and consistent with the rationale outlined in Aulbach et al. (2020), we use an average modal proportion of garnet to clinopyroxene of 55:45 in bimineralic and kyanite bearing eclogites and we consider these estimates for reconstructing the whole rock compositions. Table S1 in the ESM1 provides a detailed petrographic description of each sample along with visually estimated mineral modes.

Reconstructed whole-rock compositions

As is customary, bulk rock compositions of xenoliths are reconstructed using the constituent mineral compositions and modal estimations, which is designed to avoid the effects of melt infiltration during their entrainment in the host kimberlite (Jerde et al. 1993; Barth et al. 2001; Heaman et al. 2006; Jacob et al. 2009), and in our study further avoids

Table 2 Average major compositions, and calculated mineral formulae and nomina end-member fractions of garnet in eclogite xenoliths from the Eastern Dharwar craton

Sample	P3-10		KL2-G1		KL2-G2		KL2-G3		KL2-B1		KL-3-EC-G13		KL3-L		KL3-S		KL4-D2-6		KL2-B1a		KL4 D2-6a	
Analysis number	24		3		2		2		5		3		13		3		8		2		1	
	Content	Error	Content	Error	Content	Error	Content	Error	Content	Error	Content	Error	Content	Error	Content	Error	Content	Error	Content	Error	Content	Error
Main oxides (wt%):																						
SiO_2	39.68	(0.43)	40.14	(0.24)	40.57	(0.08)	40.52	(0.23)	39.71	(0.06)	39.68	(0.18)	41.23	(0.56)	39.81	(0.05)	39.59	(0.38)	37.5	(0.46)	37.27	
TiO_2	0.23	(0.02)	0.10	(0.03)	0.08	(0.07)	0.15	(0.03)	0.15	(0.02)	0.23	(0.02)	0.16	(0.03)	0.13	(0.02)	0.14	(0.02)	0.005	(0.01)	0.01	
Cr_2O_3	0.03	(0.01)	0.07	(0.06)	0.09	(0.07)	0.07	(0.05)	0.03	(0.01)	0.02	(0.01)	0.07	(0.04)	0.05	(0.02)	0.01	(0.01)	0.01	(0.00)	0.01	
Al_2O_3	22.18	(0.26)	22.39	(0.18)	22.52	(0.04)	22.68	(0.25)	22.25	(0.14)	22.31	(0.11)	23.01	(0.19)	22.47	(0.09)	22.21	(0.20)	22.22	(0.03)	22.46	
FeO	19.06	(0.24)	10.26	(0.67)	9.30	(0.03)	12.65	(0.59)	11.75	(0.08)	16.16	(0.05)	10.83	(0.49)	11.81	(0.12)	12.84	(0.26)	0.55	(0.02)	1.24	
MnO	0.34	(0.02)	0.28	(0.28)	0.25	(0.06)	0.16	(0.01)	0.32	(0.02)	0.29	(0.02)	0.19	(0.06)	0.26	(0.02)	0.3	(0.21)	0.005	(0.01)	0.01	
MgO	10.27	(0.17)	9.58	(0.10)	12.58	(0.01)	12.38	(0.10)	7.29	(0.01)	9.21	(0.08)	14.55	(0.32)	8.4	(0.03)	9.72	(0.12)	0.03	(0.00)	0.02	
CaO	8.13	(0.39)	15.63	(0.15)	12.66	(0.06)	10.19	(0.23)	18.49	(0.12)	12.23	(0.04)	9.88	(0.26)	17.28	(0.02)	14.24	(0.39)	38.5	(0.03)	38.19	
Na_2O	0.10	(0.01)	0.05	(0.03)	0.04	(0.01)	0.11	(0.04)	0.06	(0.01)	0.10	(0.02)	0.07	(0.02)	0.04	(0.01)	0.05	(0.01)	0.005	(0.01)	0.01	
K_2O	0.005	(0.01)	0.01	(0.01)	b.d.l.	(0.00)	b.d.l.	(0.00)	0.008	(0.00)	0.008	(0.00)	0.007	(0.01)	b.d.l.	(0.00)	0.005	(0.01)	b.d.l.	(0.00)	0.01	
Total	100.03		98.51		98.09		98.91		100.05		100.26		100.04		100.25		99.14		98.83		99.23	
Calculated mineral formulae (apfu)*:																						
Si	2.99		3.01		3.01		3.01		2.98		2.98		3.00		2.9		2.98		2.88		2.86	
Ti	0.01		0.005		0.004		0.008		0.008		0.01		0.009		0.007		0.008		0.0002		0.0005	
Al	1.97		1.98		1.97		1.98		1.96		1.97		1.97		1.97		1.97		2.01		2.03	
Fe	1.20		0.64		0.57		0.78		0.73		1.01		0.65		0.73		0.80		0.03		0.07	
Mn	0.02		0.01		0.01		0.01		0.02		0.01		0.01		0.01		0.01		0.0003		0.0006	
Mg	1.15		1.07		1.39		1.37		0.81		1.03		1.57		0.93		1.09		0.003		0.002	
Ca	0.65		1.25		1.008		0.81		1.48		0.98		0.77		1.38		1.14		3.17		3.14	
Cr	0.001		0.002		0.002		0.002		0.0008		0.0007		0.002		0.001		0.0005		0.0003		0.0003	
Na	0.007		0.003		0.002		0.007		0.004		0.007		0.005		0.002		0.004		0.0003		0.0007	
K	0.0003		0.0004		0.0004		0.0004		0.0003		0.0003		0.0003		0.0001		0.0002		0.0004		0.0004	
Sum	8.01		7.99		7.99		7.99		8.02		8.02		8.01		8.03		8.03		8.10		8.12	
Mg#	0.48		0.62		0.70		0.63		0.52		0.50		0.70		0.55		0.57		0.08		0.02	
Ca#	0.21		0.42		0.33		0.27		0.48		0.32		0.25		0.45		0.37		0.98		0.97	
Cr#	0.0005		0.001		0.001		0.001		0.0004		0.0004		0.001		0.0007		0.0002		0.0003		0.0001	
Calculated nominal mineral fractions (mol%):																						
Py	36.8		34.9		45.2		44.8		25.7		32.4		51.2		29		34.2		0.1		0.1	
Alm	36.4		21		18.8		25.7		20.4		29.2		20.3		19		22.3		0		0	
Grs	20.9		41		32.7		26.5		46.9		30.9		25		43		36		91.4		90.9	

Errors are quoted at the 1*s* level

b.d.l. = below detection limit

* Calculated based on 12 O atoms per formula unit

Mg# = molar Mg/(Mg+Fe)

Ca# = molar Ca/(Mg+Fe+Ca+Mn)

Cr# = molar Cr/(Cr+Al)

Table 3 Average trace element compositions of garnet in eclogite xenoliths from the Eastern Dharwar craton

Sample	P3-10		KL2-G1		KL2-G2		KL2-G3		KL2-B1		KL-3-EC-G13		KL3-L		KL3-S		KL4-D2-6		
Analysis number	7		1		1		1		9		11		9		10		12		
	Content	Error	Content	Error	Content	Error	Content	Error	Content	Error	Content	Error	Content	Error	Content	Error	Content	Error	Average detection limit
Sc	52	(5)	351	n.a	215	n.a	22	n.a	58	(1)	41	(2)	34	(0.58)	41	(0.23)	47	(17)	0.15
V	96	(5)	934	n.a	460	n.a	35	n.a	966	(0.78)	1933	(2.71)	1137	(3.41)	58	(1)	1017	(13)	0.03
Ti	1617	(131)	874	n.a	6610	n.a	830	n.a	74	(12)	75	(79)	65	(42)	940	(21)	53	(753)	0.79
Co	99	(9)	114	n.a	171	n.a	35	n.a	58	(5)	74	(4)	44	(4)	67	(6)	50	(17)	10
Ni	29	(1)	252	n.a	214	n.a	31	n.a	20	(0.43)	19	(1)	89	(1)	34	(0.75)	15	(4)	1.09
Cu	0.02	(0.10)	b.d.l.	n.a	5.8	n.a	0.81	n.a	0.37	(0.08)	b.d.l.	n.a	0.45	(0.28)	0.56	(0.27)	0.37	(0.20)	0.001
Ga	9.42	(0.30)	13	n.a	31	n.a	4.00	n.a	9.61	(0.25)	8.94	(0.27)	8.18	(0.26)	9.30	(0.24)	6.85	(0.92)	0.04
Ge	1.95	(0.16)	5.14	n.a	3.96	n.a	0.65	n.a	1.91	(0.18)	1.64	(0.13)	1.42	(0.12)	1.59	(0.16)	1.34	(0.41)	0.255
Rb	0.008	(0.04)	b.d.l.	n.a	b.d.l.	n.a	b.d.l.	n.a	b.d.l.	(0.01)	b.d.l.	n.a	0.01	(0.002)	b.d.l.	n.a	b.d.l.	n.a	0.0002
Sr	0.97	(0.57)	1.24	n.a	b.d.l.	n.a	0.64	n.a	4.66	(0.68)	4.16	(0.59)	2.09	(0.28)	6.56	(0.99)	3.20	(1)	0.57
Y	33	(1)	4.46	n.a	67	n.a	18	n.a	9.46	(0.24)	11	(1)	6.24	(0.28)	6.48	(0.09)	9.74	(7)	0.004
Zr	28	(3)	14.67	n.a	101	n.a	17	n.a	3.15	(0.04)	10	(1)	8.33	(2)	2.77	(0.73)	25	(78)	0.01
Nb	0.03	(0.006)	4.45	n.a	0.91	n.a	b.d.l.	n.a	0.02	(0.006)	0.01	(0.006)	0.008	(0.005)	0.03	(0.06)	0.05	(0.13)	0.004
Cs	0.03	(0.03)	b.d.l.	n.a	b.d.l.	n.a	b.d.l.	n.a	b.d.l.	n.a	b.d.l.	n.a	b.d.l.	n.a	b.d.l.	n.a	b.d.l.	n.a	0.002
Ba	0.15	(0.04)	b.d.l.	n.a	b.d.l.	n.a	b.d.l.	n.a	0.03	(0.006)	b.d.l.	n.a	b.d.l.	n.a	0.12	(0.004)	b.d.l.	n.a	0.01
La	0.0	(0.01)	0.174	n.a	0.04	n.a	0.007	n.a	0.04	(0.02)	0.04	(0.003)	0.02	(0.004)	0.10	(0.04)	0.05	(0.05)	0.005
Ce	0.12	(0.03)	1.8	n.a	0.75	n.a	0.04	n.a	0.53	(0.14)	0.59	(0.03)	0.29	(0.037)	1.08	(0.24)	0.58	(0.35)	0.003
Pr	0.05	(0.005)	0.66	n.a	0.34	n.a	0.01	n.a	0.20	(0.015)	0.23	(0.01)	0.13	(0.008)	0.30	(0.04)	0.17	(0.05)	0.001
Nd	0.72	(0.04)	7.01	n.a	3.85	n.a	0.24	n.a	1.85	(0.05)	2.53	(0.17)	1.61	(0.11)	1.90	(0.16)	1.40	(0.14)	0.01
Sm	0.97	(0.03)	2.81	n.a	2.90	n.a	0.41	n.a	0.90	(0.03)	1.71	(0.15)	1.27	(0.10)	0.65	(0.03)	0.82	(0.29)	0.014
Eu	0.65	(0.06)	0.678	n.a	1.21	n.a	0.25	n.a	0.89	(0.02)	1.17	(0.08)	0.86	(0.03)	0.77	(0.02)	0.60	(0.10)	0.012
Gd	2.81	(0.23)	1.53	n.a	4.95	n.a	1.33	n.a	1.27	(0.11)	2.39	(0.35)	1.44	(0.23)	0.89	(0.03)	1.35	(0.82)	0.08
Tb	0.71	(0.02)	0.14	n.a	1.15	n.a	0.32	n.a	0.23	(0.008)	0.37	(0.06)	0.19	(0.03)	0.15	(0.004)	0.26	(0.19)	0.002
Dy	5.83	(0.17)	0.82	n.a	10	n.a	2.86	n.a	1.68	(0.05)	2.26	(0.36)	1.18	(0.09)	1.13	(0.02)	1.81	(1.44)	0.009
Ho	1.36	(0.09)	0.17	n.a	2.53	n.a	0.7	n.a	0.37	(0.01)	0.42	(0.06)	0.23	(0.01)	0.25	(0.007)	0.38	(0.29)	0.002
Er	4.19	(0.36)	0.52	n.a	8.17	n.a	2.20	n.a	1.12	(0.04)	1.09	(0.15)	0.70	(0.02)	0.76	(0.01)	1.08	(0.80)	0.003
Tm	0.59	(0.05)	0.08	n.a	1.25	n.a	0.34	n.a	0.16	(0.005)	0.13	(0.01)	0.09	(0.003)	0.11	(0.003)	0.14	(0.10)	0.001
Yb	4.17	(0.51)	0.72	n.a	8.48	n.a	2.36	n.a	1.16	(0.05)	0.91	(0.14)	0.69	(0.016)	0.82	(0.01)	0.99	(0.61)	0.01
Lu	0.62	(0.07)	0.13	n.a	1.33	n.a	0.36	n.a	0.17	(0.005)	0.13	(0.01)	0.10	(0.003)	0.12	(0.004)	0.14	(0.07)	0.001
Hf	0.38	(0.04)	0.32	n.a	1.78	n.a	0.19	n.a	0.07	(0.004)	0.13	(0.009)	0.11	(0.02)	0.06	(0.008)	0.49	(1.49)	0.004
Ta	0.001	(0.0005)	0.33	n.a	0.09	n.a	b.d.l.	n.a	0.0008	(0.0004)	0.0007	(0.0004)	0.0004	(0.0003)	b.d.l.	(0.0002)	0.04	(0.06)	0.0001
Pb	b.d.l.	(0.003)	0.34	n.a	0.38	n.a	0.07	n.a	b.d.l.	(0.002)	0.004	(0.003)	0.003	(0.001)	0.005	(0.009)	0.004	(0.004)	0.01
Th	0.001	(0.002)	0.08	n.a	0.01	n.a	0.004	n.a	0.005	(0.001)	0.003	(0.0007)	0.001	(0.0004)	0.01	(0.01)	0.02	(0.02)	0.0003
U	0.002	(0.0003)	0.13	n.a	0.04	n.a	0.009	n.a	0.006	(0.002)	0.01	(0.003)	0.005	(0.002)	0.07	(0.04)	0.06	(0.08)	0.0004

All values are quoted in ppm, and errors are quoted at the 1*s* level

b.d.l.= below detection limit

n.a=not available

Table 4 Average major compositions, and calculated mineral formulae and nomina end-member fractions of clinopyroxene in eclogite xenoliths from the Eastern Dharwar craton

Sample	P3-10		KL2-B1		KL3-L		KL3-S		KL-3-EC-G13		KL4-D2-6	
Analysis number	3		3		3		3		2		11	
	Content	Error	Content	Error	Content	Error	Content	Error	Content	Error	Content	Error
Main oxides (wt%):												
SiO_2	54.62	(0.30)	54.45	(0.92)	51.46	(0.46)	50.81	(0.62)	55.09	(0.07)	54.25	(0.14)
TiO_2	0.52	(0.04)	0.14	(0.04)	0.39	(0.30)	0.04	(0.04)	0.31	(0.01)	0.18	(0.02)
Cr_2O_3	0.07	(0.05)	0.05	(0.02)	0.10	(0.03)	0.06	(0.04)	0.04	(0.01)	0.03	(0.01)
Al_2O_3	8.49	(0.24)	12.17	(0.39)	10.48	(0.32)	11.47	(0.89)	14.52	(0.01)	14.43	(0.09)
FeO	2.75	(0.21)	1.86	(0.14)	1.90	(0.22)	2.80	(0.89)	3.10	(0.01)	2.45	(0.08)
MnO	0.20	(0.10)	0.10	(0.04)	0.02	(0.02)	0.01	(0.00)	0.03	(0.01)	0.02	(0.01)
MgO	11.59	(0.48)	9.42	(0.34)	8.89	(0.40)	11.25	(0.72)	7.26	(0.01)	7.74	(0.07)
CaO	19.02	(0.81)	14.85	(0.38)	17.56	(0.50)	16.44	(0.42)	12.72	(0.04)	13.77	(0.09)
Na_2O	3.22	(0.79)	6.61	(0.28)	3.38	(0.53)	5.77	(0.18)	6.71	(0.01)	6.11	(0.05)
K_2O	0.01	(0.00)	0.02	(0.00)	1.78	(0.51)	0.02	(0.00)	0.06	(0.00)	0.04	(0.01)
BaO	0.01	(0.01)	0.004	(0.00)	3.20	(0.25)	1.68	(0.45)	b.d.l	(0.00)	b.d.l	(0.00)
Total	100.50		99.67		99.16		100.35		99.83		99.04	
Calculated mineral formulae (apfu)*:												
Si	1.96		1.92		1.93		1.81		1.96		1.94	
Ti	0.014		0.004		0.011		0.001		0.008		0.005	
Cr	0.002		0.001		0.003		0.002		0.001		0.001	
Al	0.36		0.51		0.46		0.48		0.61		0.61	
Fe	0.082		0.055		0.061		0.083		0.092		0.073	
Mn	0.006		0.003		0.001		0.001		0.001		0.001	
Mg	0.62		0.50		0.50		0.60		0.38		0.41	
Ca	0.73		0.56		0.71		0.63		0.48		0.53	
Na	0.22		0.45		0.25		0.40		0.46		0.42	
K	0.001		0.001		0.085		0.001		0.003		0.002	
Sum	4.00		4.00		4.00		4.00		4.00		4.00	
Mg#	0.88		0.90		0.89		0.88		0.81		0.85	
Ca#	0.51		0.50		0.56		0.48		0.50		0.52	
Cr#	0.01		0.002		0.01		0.004		0.002		0.002	
Calculated nominal mineral fractions (mol%):												
Jd	22.50		42.80		33.10		29.10		46.50		42.60	
Molar Na/(Na+Ca)	0.23		0.45		0.26		0.39		0.49		0.44	

Errors are quoted at the 1*s* level

b.d.l. = below detection limit

* Calculated based on 6 O atoms per formula unit

Mg# = molar Mg/(Mg+Fe)

Ca# = molar Ca/(Mg+Fe+Ca+Mn)

Cr# = molar Cr/(Cr+Al)

Table 5 Average major and trace element compositions of kyanite in eclogite xenoliths from the Eastern Dharwar craton

Sample	KL2-B1		KL3-S	KL4-D2-6	
Analysis number	5		1	5	
	Content	Error	Content	Content	Error
Main oxides (wt%):					
SiO_2	37.19	(0.45)	37.60	36.76	(0.18)
TiO_2	0.04	(0.02)	0.05	0.04	(0.02)
Cr_2O_3	0.06	(0.01)	0.07	0.04	(0.02)
Al_2O_3	61.85	(0.24)	62.13	61.64	(0.42)
FeO	0.27	(0.03)	0.21	0.22	(0.08)
MnO	0.01	(0.01)	0.01	0.004	(0.01)
MgO	0.03	(0.01)	0.05	0.03	(0.01)
CaO	0.15	(0.21)	0.06	0.01	(0.01)
Na_2O	0.002	(0.00)	0.06	0.01	(0.01)
K_2O	0.01	(0.01)	0.05	0.003	(0.01)
Total	99.61		100.273	98.75	
Trace elements (ppm):					
Analysis number	1		1	1	Average detection limit
Ba	44		47	39	0.0207
Sc	2.75		3.77	3.79	0.17
Ti	348		328	317	0.81
V	58		65	52	0.08
Cr	668		246	298	1.69
Ni	1.99		2.90	2.79	0.60
Sr	0.89		0.72	0.70	0.31

Errors are quoted at the 1*s* level

extensive secondary alteration. A comprehensive review of modal abundances in larger eclogite xenoliths (> 10 cm) and experimental studies exploring phase relationships in eclogites with mid-oceanic ridge basalts (MORB) composition (i.e. the assumed protolith; Jacob 2004; Aulbach and Jacob 2016) suggests garnet-clinopyroxene proportions of 55 and 45 wt%, respectively, with total uncertainties in modal abundances estimated at 10% (Aulbach et al. 2020). In contrast, for kyanite-bearing eclogites, modal proportions were established using visual estimates, as described in Table S1 in the ESM1, to calculate the bulk compositions of major elements. The reconstructed bulk rock compositions are represented in Tables 6 and 7.

The reconstructed bulk major element compositions of the Dharwar eclogites show Mg# values ranging from 0.59 to 0.76, which is consistent with previous studies (Dongre et al. 2015; Shaikh et al. 2023). Bulk CaO values are high, ranging from 12.45% to 16.52 wt%. However, compared to modern MORB (GEOROC: https://georoc.mpch-mainz.gwdg.de; accessed 19 April 2025), the eclogites generally exhibit a lower range of SiO_2 (44.53–46.62 wt% vs. 49–52 wt%) and FeO (6.81–11.72 wt% vs. 7–12 wt%), while their ranges of CaO (12.45–16.52 wt% vs. 13–17 wt%) and MgO (8.33–11.90 wt% vs. 6–10 wt%) are similar. The latter places their bulk major element compositions predominantly in the basaltic (8.08 to 11.90 wt% MgO) rather than picritic range (> 12 wt% MgO) (Hills and Haggerty 1989; Jacob and Foley 1999; Barth et al. 2002; Schmickler et al. 2004; Tappe et al. 2011). The lower FeO content is a characteristic of gabbroic eclogites and is attributed to accumulation of minerals enriched in FeO and its incompatibility during magmatic processes (Aulbach et al. 2020). Bulk TiO_2 concentrations are generally low (0.09 to 0.36 wt%), which may partly reflect that the abundance of accessory rutile is not considered in the reconstruction, with the exception of rutile-bearing sample (P3-10) with 0.36 wt% TiO_2.

The reconstructed whole-rock chondrite-normalized spidergrams indicate a range from depletion (Sm_N/La_N = 1.23 to 3.00) in LREE to slightly decreasing to flat HREE (Lu_N/Gd_N = 0.52 to 1.83) patterns (Fig. 5c). Europium and Sr are enriched relative to adjacent REE; as these elements have similar compatibility to adjacent REE, they are not expected to be enriched during peridotite melting (Fig. 5d). Positive Sr anomalies are expressed as high Sr_N/Nd_N values, ranging from 3.39 to 6.51. Comparing trace element patterns with those from previous studies for the Dharwar craton eclogite xenoliths (Dongre et al. 2015), our findings are consistent overall, except for relatively lower HREE concentrations (subchondritic) observed in Group 1 eclogites in the earlier study. The trace element patterns align with the range of compositions reported for Phanerozoic gabbros, including olivine gabbros, troctolitic gabbros, and gabbro norites (Fig. 5d).

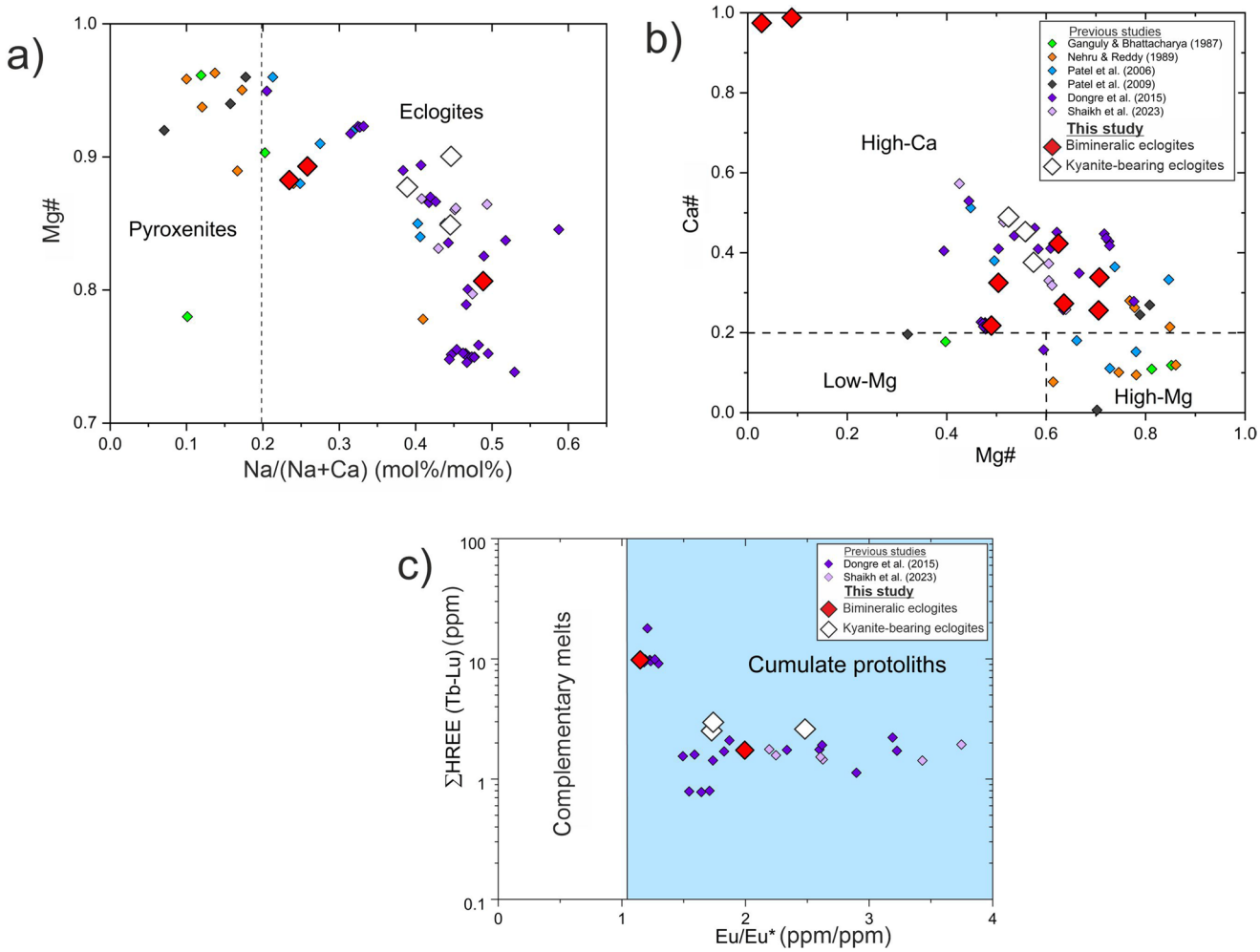


Fig. 4 (**a**) Mg# [molar Mg/(Mg+Fe_{total})] as a function of molar Na/(Na+Ca) in clinopyroxene, separating pyroxenites from eclogites, for samples in the present and previous studies reported from the Eastern Dharwar craton. Clinopyroxenes with molar Na/(Na+Ca)>0.2 correspond to eclogites (simplified classification; see Aulbach and Jacob 2016). (**b**) Ca# [molar Ca/(Ca+Fe+Mg+Mn)] shown as a function of Mg# in eclogitic garnets from the present study compared with previous studies (cited in the legend) from the Eastern Dharwar craton. Fields of low-Mg, high-Mg and high-Ca garnets are after Aulbach and Jacob (2016). (**c**) Total HREE content as a function of Eu/Eu* [=Eu_N/(Sm_N×Gd_N)0.5; where the subscript N denotes chondrite-normalised (McDonough and Sun 1995) mass fractions] in eclogites from the present study compared with the previous studies from the Eastern Dharwar craton. Eu/Eu* >1.05 is interpreted as reflecting a gabbroic cumulate protolith, and Eu/Eu* <1.05 as complementary residual melt protoliths (after Aulbach and Jacob 2016), but may also reflect muting of cumulate protolith signatures due to mantle metasomatism (Aulbach et al. 2020)

Geothermobarometry

Equilibrium temperatures and pressures in eclogite samples were estimated based on the chemical compositions of coexisting garnet and omphacitic clinopyroxene. The absence of tetrahedrally coordinated aluminium in clinopyroxene, a pressure-sensitive indicator, complicates barometric measurements for mantle eclogites (Beyer et al. 2015). Therefore, in keeping with prior work (Aulbach et al. 2020), the garnet-clinopyroxene Fe^{2+}-Mg exchange geothermometer proposed by Krogh (1988) was employed to obtain temperatures which were solved iteratively with the regional steady-state conductive geotherm of 40 mW/m² from the Dharwar craton (Karmalkar et al. 2009; Shaikh et al. 2023). These estimates may be influenced by uncertainties linked to advective heating (i.e. non-equilibration to a regional steady-state geotherm), but nonetheless remain the best approach for eclogite xenoliths (H. Grütter, *pers. comm.*). The temperatures range from 726 to 1122 °C, with bimineralic and kyanite-bearing eclogites representing the lower and upper-temperature extremes, respectively. The estimated equilibrium pressures for the eclogite samples vary between 2.6 and 4.8 GPa. These values are in close agreement with previous results on mantle xenoliths (Fig. 6)

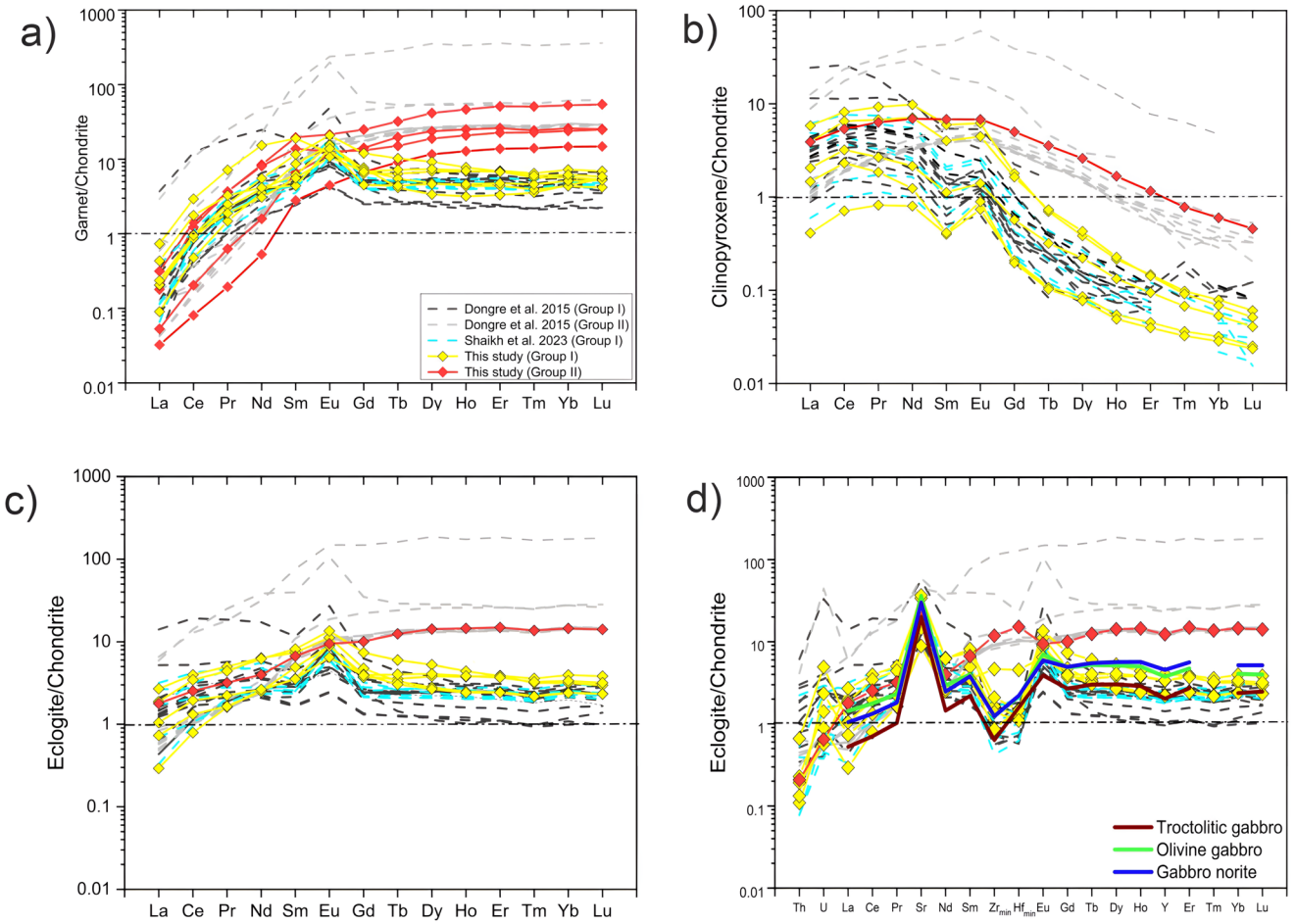


Fig. 5 Chondrite-normalized (**a**) REE patterns of Group I and II eclogitic garnets, (**b**) REE patterns of Group I and II eclogitic clinopyroxenes, (**c**) REE patterns of reconstructed bulk eclogite xenoliths from the Eastern Dharwar craton, (**d**) Trace element patterns of reconstructed bulk eclogite xenoliths from the Eastern Dharwar craton. Patterns of average troctolitic gabbros, average olivine gabbro and gabbro norite from Benoit et al. (1996) are plotted for reference. Note that Zr and Hf abundances in the reconstructed bulk rocks are minima since rutile, as a major HFSE host, was not considered

Table 6 Average reconstructed bulk-rock major element (wt%) compositions of eclogite xenoliths from the Eastern Dharwar craton

Sample	P3-10	KL2-B1	KL3-L	KL3-S	KL3-EC-G13	KL4-D2-6
SiO_2	46.40	46.14	45.84	44.53	46.62	46.09
TiO_2	0.36	0.14	0.27	0.09	0.27	0.16
Cr_2O_3	0.05	0.04	0.09	0.06	0.03	0.02
Al_2O_3	16.02	18.61	17.38	18.87	18.81	19.14
FeO	11.72	7.17	6.81	7.54	10.28	8.09
MnO	0.28	0.21	0.11	0.14	0.17	0.17
MgO	10.86	8.08	11.90	9.39	8.33	8.75
CaO	13.03	16.52	13.34	16.40	12.45	13.89
Na_2O	1.50	2.94	1.56	2.53	3.08	2.75
K_2O	0.01	0.01	0.81	0.01	0.03	0.02
BaO	0.003	b.d.l	1.44	0.73	b.d.l	b.d.l
Total	100.25	99.88	99.65	100.29	100.06	99.09
Mg#	0.62	0.67	0.76	0.69	0.59	0.66
CaO/Al_2O_3	0.81	0.89	0.77	0.87	0.66	0.73

b.d.l.= below detection limit

Mg# = molar Mg/(Mg + Fe)

Reconstructed whole-rock compositions were calculated using visual mineral mode estimates provided in Appendix 1 (Supplementary file 1)

Table 7 Average reconstructed bulk-rock trace element (ppm) compositions of eclogite xenoliths from the Eastern Dharwar craton

Sample	P3-10	KL2-B1	KL3-L	KL3-S	KL3-EC-G13	KL4-D2-6
Sc	40	41	23	24	27	31
Sr	152	64	246	119	266	105
Y	19	5.25	3.55	3.46	6.35	5.31
Zr	45	3.30	6.27	5.30	8.0	18
La	0.42	0.07	0.64	0.17	0.45	0.25
Ce	1.55	0.49	2.43	0.81	2.12	1.20
Pr	0.30	0.15	0.46	0.15	0.41	0.21
Nd	1.82	1.19	2.91	1.14	2.85	1.21
Sm	0.99	0.53	1.10	0.73	1.21	0.52
Eu	0.53	0.51	0.63	0.50	0.76	0.36
Gd	2.0	0.74	0.94	0.80	1.47	0.78
Tb	0.45	0.13	0.12	0.11	0.22	0.15
Dy	3.50	0.94	0.69	0.66	1.30	1.0
Ho	0.79	0.21	0.14	0.13	0.24	0.21
Er	2.39	0.62	0.40	0.39	0.62	0.59
Tm	0.34	0.09	0.05	0.05	0.08	0.08
Yb	2.34	0.64	0.39	0.39	0.51	0.54
Lu	0.35	0.09	0.06	0.06	0.07	0.08
Hf	1.56	0.15	0.13	0.11	0.15	0.47
Th	0.01	0.003	0.01	0.004	0.01	0.02
U	0.005	0.01	0.004	0.02	0.01	0.04

Reconstructed whole-rock compositions were calculated using visual mineral mode estimates provided in Appendix 1 (Supplementary file 1)

(Karmalkar et al. 2009). Temperatures for garnet separates from peridotite xenoliths were determined using the Ni in garnet thermometer (Sudholz et al. 2021), yielding a range of 1013 to 1243 °C. Pressure estimates were again derived by projecting these temperatures onto the Dharwar cratonic geotherm, as described above. The calculated pressures fall within the range of 4.2 to 5.5 GPa.

The original residence depths of the samples in the lithospheric mantle, prior to their entrainment in the host kimberlite around 1100 Ma, were estimated using a well-established equation [$Z = (P - 13.7) \times 3.092 + 50$], derived from numerical models and peridotite xenolith data from the Fennoscandian Shield (Kukkonen et al. 2003). According to these calculations, the Dharwar eclogites equilibrated at depths ranging from 85 to 153 km, whereas the peridotitic garnet samples originated at depths of 135 to 175 km.

Ferric over total iron ratios in Garnet and Estimation of oxygen fugacity (fO_2)

In peridotitic garnet separates, the $Fe^{3+}/\Sigma Fe$ ratios range from 0.05 to 0.18, while the eclogitic garnet separate yields a ratio of 0.06. Using the oxybarometer developed by Stagno et al. (2013), the oxygen fugacity [$\Delta \log fO_2$ (FMQ)] of the peridotitic garnet separations was determined, aligning with previous reports within an estimated error range of ± 0.9 log units. The Fe# values for olivine and orthopyroxene used in calculating the $\Delta \log fO_2$ were derived from the mineral compositions reported by Pattnaik et al. (2020). The calculated $\Delta \log fO_2$ values for the peridotitic garnets range from − 3.4 to -4.3 FMQ (Table S14 in the ESM1). For the eclogitic garnet (KL2), the oxygen fugacity was assessed using the oxybarometer devised by Stagno et al. (2015). The resulting $\Delta \log fO_2$ value for KL2 was − 0.03 FMQ, with a calibration-related error estimate of ± 0.6 log units (Table S14 in the ESM1). This calculation considered the observed chemical compositions of garnet and clinopyroxene, along with the pressure-temperature conditions derived from the samples.

Estimation of mass density and seismic velocity in Dharwar mantle xenoliths

Physical properties such as mass densities (rho) ranging from 3.56 to 3.62 g/cm³, and seismic velocities including P-wave velocities (V_P) between 8.46 and 8.63 km/s, and S-wave velocities (V_S) between 4.80 and 4.91 km/s, were computed from the spreadsheet of Abers and Hacker (2016) (Table 1), using the pressures and temperatures obtained as described above, and garnet and clinopyroxene compositions reported in Tables 2 and 4. For the previously reported peridotite xenoliths from the EDC by Pattnaik et al. 2020; the mass densities and seismic velocities were also computed and compared to the eclogites. Further, as a reference for an intact cratonic lithosphere, mass densities and S-wave velocities for the peridotites from the Siberian craton were also calculated and based on data reported in earlier studies

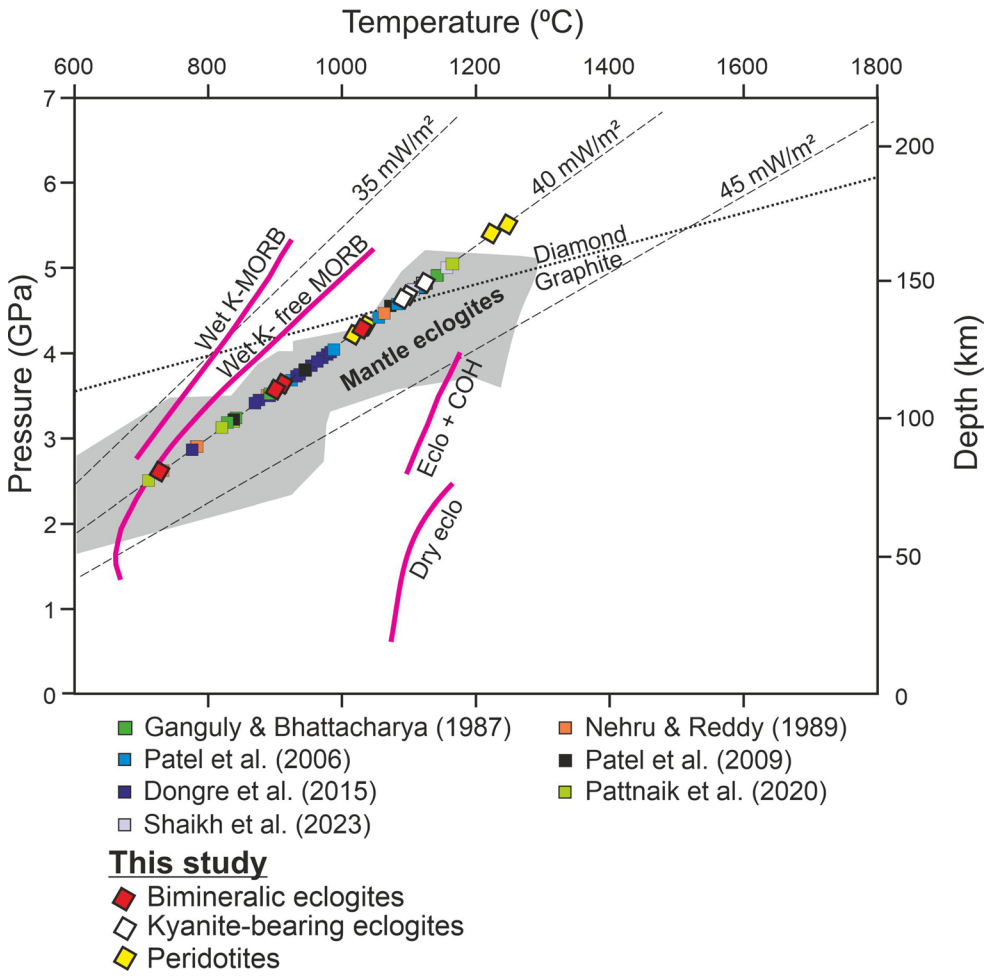


Fig. 6 Equilibrium pressure (P)-temperature (T) plot for eclogite xenoliths and peridotite xenocrysts in kimberlites from the Eastern Dharwar craton. Temperatures are calculated using the clinopyroxene-garnet Fe-Mg exchange thermometer of Krogh (1988) for eclogites and Ni in garnet thermometer of Sudholz et al. (2021) for the garnet separates from peridotite xenoliths; pressures are calculated by projecting the respective temperatures onto the Dharwar geotherm (assumed as 40 mW/m^2 after Dongre et al. 2015; Shaikh et al. 2023). The continental geotherms from 35 to 45 mW/m^2 (Hasterok and Chapman 2011) are shown as grey dashed lines. The graphite-diamond transition (Day 2012) is shown as a black dashed line for reference. Estimates of P-T conditions of equilibrium from previous studies for mantle eclogite and peridotite xenoliths from the Eastern Dharwar craton are also shown for comparison. The grey field is after Aulbach (2020) for mantle eclogite xenoliths world-wide. Wet K-bearing and K-free MORB solidi (thick pink lines) from Schmidt and Poli (2013) and solidus for dry melting of reduced eclogite + COH from Litasov et al. (2014) illustrating that most eclogite xenoliths from the Eastern Dharwar craton would have lost a partial melt if they contained sufficient water during subduction (Dongre et al. 2015)

from the region (Boyd 1984; Sobolev et al. 1984; Boyd et al. 1997; Doucet et al. 2012, 2013; Ionov et al. 2015, 2018, 2020; Goncharov et al. 2012; Agashev et al. 2013; Liu et al. 2022).

Discussion

Origin and metamorphic-metasomatic evolution of the Dharwar eclogites

The low-pressure origin as subducted oceanic crust and subsequent metamorphism of eclogite xenoliths from Dharwar have been well delineated (Dongre et al. 2015), providing an important framework within which to examine the physical properties and late-stage mineralogical-compositional evolution of the eclogite reservoir in this craton that are the focus of the present study. Based on major and trace element characteristics, Dongre et al. (2015) identified two groups of eclogites, of which one shows strong Eu and Sr anomalies [characterized by Sr/Sr* ratios (chondrite-normalized Sr*= Sr/(Pr*Nd)^0.5; chondrite of Sun and McDonough 1989] along with low total REE contents characteristic of gabbroic lower oceanic crust, and the other one has negative anomalies and higher REE contents, but higher, supra-mantle $\delta^{18}O$ values typical of upper portions of seawater-altered oceanic crust, firmly establishing their subduction origin.

The eclogite samples studied here also have prominent positive Sr and Eu anomalies in the bulk rocks and minerals (Figs. 4c and 5d) and flat HREE patterns, suggesting an origin from cumulate plagioclase-rich plutonic rocks which initially formed in oceanic crustal magma chambers (Jacob and Foley 1999), consistent also with high normative plagioclase modes (50%; Johannsen 1937) in the reconstructed whole rocks (Table S10 in the ESM1). High reconstructed bulk Al_2O_3 contents (16.02 to 19.14 wt%) and CaO contents (12.45 to 16.52 wt%) compared to the MORB compositions (Jenner and O' Neill 2012) further document the effect of cumulate plagioclase in the mafic protoliths (Taylor and Neal 1989).

The SiO_2 contents of Dharwar eclogites are lower (<47 wt%) than those of Archean basalts and modern oceanic gabbros, which is characteristic of cratonic mantle eclogites (Jacob 2004) and has been interpreted to reflect partial melt loss at the time of subduction of the ancient oceanic crust (Ireland et al. 1994; Jacob et al. 1994; Rudnick 1995; Tappe et al. 2011; Smart et al. 2014). However, especially for eclogite xenoliths with low-pressure cumulate protoliths, such as those from the Dharwar craton, LREE depletion may alternatively be the result of accumulation, with exclusion of highly incompatible elements including LREE, and does not require the loss of partial melt (Aulbach and Jacob 2016). Depleted LREE abundances also preclude significant subsequent metasomatism by incompatible element-enriched melts, consistent with their low MgO contents, which tend to increase significantly during mantle metasomatism (e.g., Barth et al. 2002). Although Sommer et al. (2017) ascribed the coexistence of bimineralic and kyanite-bearing eclogites to kyanite breakdown facilitated by heating and fluid ingress, the lower average temperatures for three bimineralic eclogites (883 °C) than for kyanite eclogites (1103 °C) seems to argue against this origin for the samples studied here. Instead, it may result from mineralogical differences in the protoliths and varying normative plagioclase modes (53 vol% for bimineralic eclogites vs.47 vol% for kyanite eclogites; Table S10 in the ESM1), if not due to the fact that kyanite abundance is low (2 vol% in the three eclogite xenoliths studied here) and may easily be missed in a given thin section.

Significance of grospyditic garnet in kyanite eclogites: evidence for decompression during pre-eruptive mantle uplift

Grospydites are a rare variety of eclogite xenoliths characterized by extremely Ca-rich compositions resulting in a mineral composition of grossular-rich garnet, jadeite-rich clinopyroxene and by the presence of kyanite (Sobolev 1968; Lappin 1978; Smyth et al. 1989), and can provide valuable insights into the metamorphic evolution of their deep cratonic mantle sources. Grospydites have been documented among a few eclogite xenoliths found in kimberlite pipes, such as Robert Victor and Kuruman in the Kaapvaal craton, and the Zagadochnaya kimberlite pipe in the Siberian craton (Sobolev 1968; Chinner and Cornell 1974; Lappin 1978; Smyth 1980; Smyth et al. 1989; Caporuscio and Smyth 1990; Schmickler et al. 2004; Marras et al. 2025).

Grospyditic garnets, with a grossular component of approximately 91%, are present in two kyanite-bearing eclogites (KL2 B1 and KL4 D2-6) from this study (Table 2). They are distinguished from other garnets by a mottled appearance, and also notable alteration in the xenolith in general, dominantly reflecting the poor stability in particular of jadeite-rich clinopyroxene in the presence of kimberlite (Fig. 3b). As importantly, kyanite is strongly associated with clinopyroxene (Fig. 3b), suggesting an origin by exsolution, which may have resulted from substantial subsolidus volume changes that led to the formation of grospyditic garnet and kyanite during re-equilibration. These textural features may have resulted from subsolidus re-equilibration due to decompression from elevated pressures. If so, this is of geodynamic importance, as it may reflect lithospheric uplift in response to thinning due to the reworking of deep cratonic roots prior to Mesoproterozoic Wajrakarur kimberlite magmatism, rather than or in addition to the thinning caused by much later Gondwana breakup (140 Ma) as suggested by Griffin et al. (2009). This uplift, in turn, can facilitate decompression melting within or below the lithospheric mantle and the generation of melts that interact with, refertilize and metasomatize the overlying lithosphere, affecting its diamond endowment and its geophysical properties, such as mass density and oxygen fugacity that will be discussed in a later section.

Celsian in kyanite eclogites related to late-stage melt infiltration

The eclogite xenoliths retained low-pressure protolith signatures and lack of evidence for mantle metasomatism that was long-lasting enough that their trace element patterns were affected. Thus, the bulk rock REE patterns show that they remain largely LREE depleted (Fig. 5d). Nevertheless, the simultaneous enrichment of LREE and MgO in a few reconstructed whole rocks (this study and published data) indicates metasomatism by a kimberlite-like melt (Fig. 7a), as is typical of eclogite xenolith suites worldwide (Aulbach et al. 2020). This kimberlite-like metasomatism is associated by a decrease in bulk-rock Eu/Eu* as MgO content increases (Fig. 7b). In this discussion, the presence of celsian in Dharwar eclogites, which has been described before (Misra et al. 2008; Dongre et al. 2015), as a secondary phase

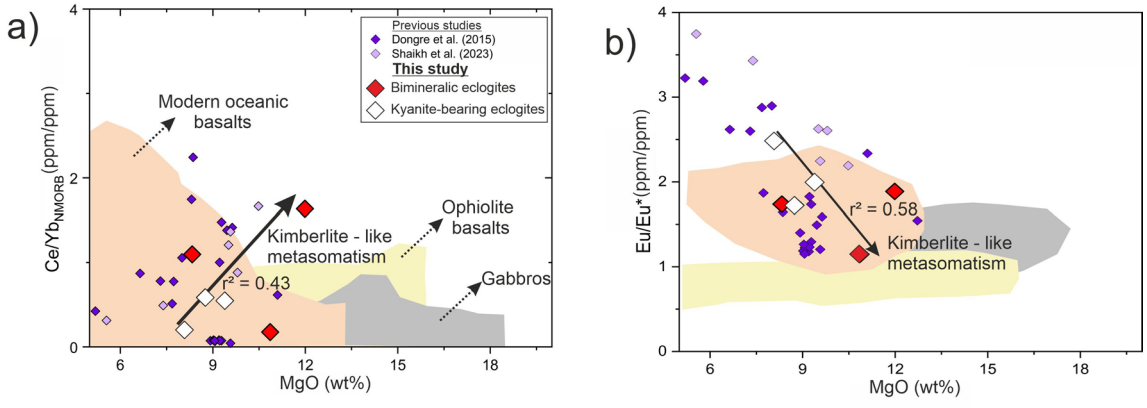


Fig. 7 (**a**) NMORB-normalized (NMORB from Gale et al. 2013) Ce/Yb plotted as a function of MgO content in reconstructed bulk eclogites of the present study and compared with the previous studies from the Eastern Dharwar craton, (**b**) Eu/Eu* plotted as a function of MgO content. Only a few samples show simultaneously high MgO contents and enrichment in LREE (expressed as Ce/Yb$_{NMORB}$ in panel a), typical of metasomatism by kimberlite-like melt, which may have reduced the size of their Eu anomaly (Aulbach et al. 2020). Data sources for fields of modern oceanic basalts and ophiolite basalts are obtained from PetDB (http://www.earthchem.org/petdb; accessed 19 April 2025), while gabbro data are from Godard et al. (2009). 'N' in NMORB refers to *normal* mid-ocean ridge basalt

in two kyanite-bearing eclogite samples (KL2-B1 and KL4-D2-6), may offer additional insights.

The occurrence of celsian, a K and Ba-rich feldspar, in eclogite xenoliths is uncommon. It has been reported in eclogite xenoliths from the Bellsbank (Taylor and Neal 1989) and Robert Victor kimberlite from South Africa (Ongley et al. 1987) and from the Lahtohjoki kimberlite pipe from Eastern Finland (Peltonen et al. 2002). McCormick et al. (1994) proposed that in Roberts Victor and Bellsbank eclogites, Ba and K found in secondary minerals were derived from clinopyroxene originally under high pressure. Conversely, Schulze and Helmstaedt (1988) attributed the occurrence of celsian feldspar, along with high-temperature sanidine, within eclogite from Roberts Victor (South Africa) to kimberlite-related metasomatism.

A mantle metasomatic vs. entrainment origin can be distinguished through detailed petrographic observations. At Dharwar, celsian typically occurs along grain boundaries, fractures, or as reaction rims (Figs. 2b, g and h and 2a and b). As observed in prior work (Dongre et al. 2015), celsian mostly appears to be replacing kyanite, but also fills in the fractures of some garnets (Figs. 2h and j and 2), both of which can furnish the Al_2O_3, but not the Ba and K necessary for celsian formation. Kelyphite rims around garnet, which result from decompression, appear to facilitate the formation of celsian (Fig. 2b), via the creation of sites for the infiltration of and reaction with Ba-K-rich fluids. Therefore, celsian is texturally younger than the kelyphite rims. As the celsian-bearing kyanite eclogites do not bear the hallmarks of mantle metasomatism (i.e. they are MgO-poor and LREE-depleted), this interaction was likely a relatively late event, related to infiltration of host kimberlite melt just prior to or during transport to the surface.

Metasomatic control on the oxygen fugacity profile beneath the Dharwar craton and its link to the regional diamond inventory

Employing Mössbauer spectroscopy (Woodland and Peltonen 1998; Woodland and Koch 2003; McCammon and Kopylova 2004; Lazarov et al. 2009) or the electron microprobe-based flank method (Höfer and Brey 2007; Creighton et al. 2009, 2010) to assess Fe^{3+} content in garnets, numerous studies consistently demonstrate a correlation between oxidation state and metasomatic enrichment in cratonic lithospheric mantle, including the Kaapvaal, Slave, Siberian cratons, and the Fennoscandian Shield.

The peridotitic garnets studied here exhibit a range of $\Delta\log fO_2$ (FMQ) values from −4.33 to -3.38, consistent with estimates by Shaikh et al. (2023), and allowing increased confidence in the fO_2 profile obtained for the regional cratonic lithosphere. The results suggest that $\Delta\log fO_2$ (FMQ) of the Dharwar peridotites roughly decreases as pressure increases, a trend that is consistent across garnet peridotite xenoliths from various cratons (Fig. 8). The correlation is attributed to the positive molar volume change associated with the fO_2 buffering reaction in garnet peridotite assemblages, which shows the primacy of garnet-based iron equilibria in controlling fO_2 in the Dharwar cratonic mantle. Nevertheless, metasomatic effects may be superposed on the primary fO_2 variation of the mantle within the EDC, which may explain the scatter in the pressure-fO_2 diagram, in particular the variable fO_2 at a given pressure (Fig. 8). Indeed, Pattnaik et al. (2020, 2021); Babu et al. (2023) and Shaikh et al. (2023) discussed the oxidative metasomatism of peridotite xenoliths from the EDC by carbonated silicate melts in the cratonic lithosphere, and inferred the diamond-destructive

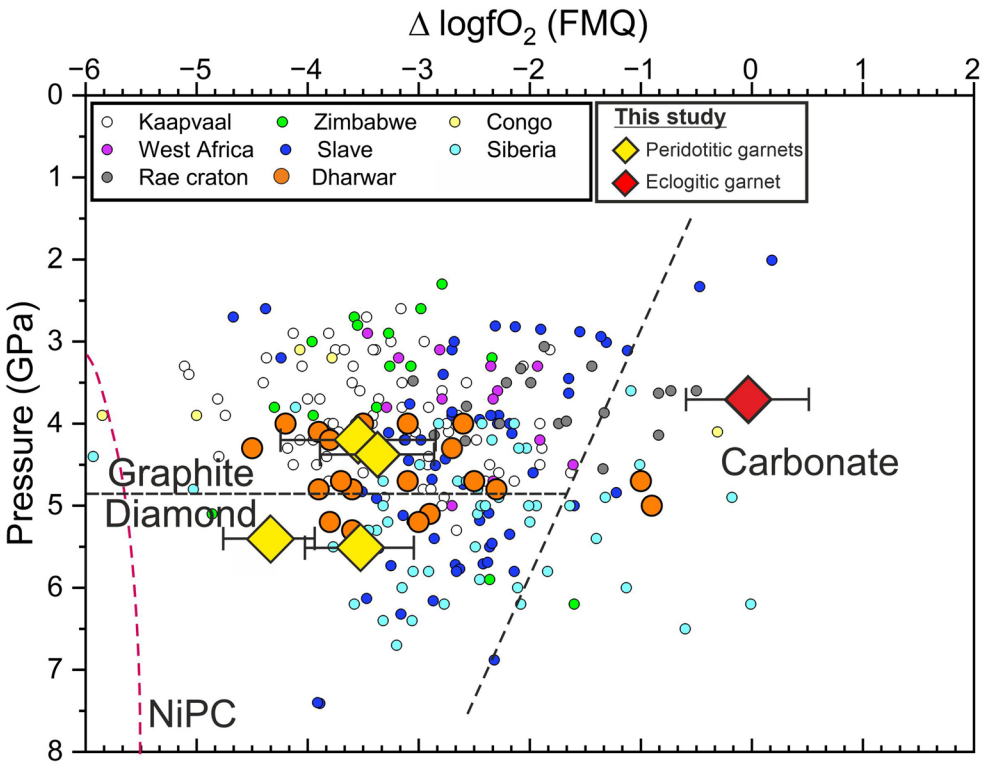


Fig. 8 $\Delta \log fO_2$ relative to the FMQ buffer calculated for peridotitic garnets (yellow diamonds) (after Stagno et al. 2013) and a single eclogitic garnet (red diamond; after Stagno et al. 2015) plotted against estimated equilibration pressures and compared with published data from the Dharwar craton (Shaikh et al. 2023) for peridotites and eclogites, as well as with data from both peridotites and eclogites from various cratons worldwide (Kaapvaal – Williams et al. 2009; Aulbach et al. 2017; Burness et al. 2020; Smart et al. 2021; Rae – Woodland et al. 2021; Slave – Smart et al. 2017; Yaxley et al. 2017; Siberia – Mikhailenko et al. 2020; West Africa – Aulbach et al. 2019; Zimbabwe – Aulbach et al. 2019; Congo – Nikitina et al. 2014; Korolev et al. 2021). Graphite-diamond-carbonate melt boundaries after Stagno et al. (2015). NiPC is the Ni precipitation curve from O'Neill and Wall (1987). Error bars represent uncertainties arising from compositional variations in olivine and orthopyroxene

nature of this process. This may be confirmed by the poorly diamondiferous nature of the P1 and P3 kimberlites (Ravi et al. 2013). Values of $\Delta \log fO_2$ (FMQ) increase with the concentrations of metasomatic indicators such as Ti/Eu, and Zr, with unclear effects on La/Yb_N, supporting the inference of oxidative melt metasomatism involving a kimberlite-like melt (Fig. 9). Contrastingly, the P7 kimberlite is diamondiferous and the peridotitic garnet separates are from a melt-depleted source (garnet $TiO_2 = 0.04$ vs. 0.16 to 0.29 wt% in garnet from the other two kimberlites). The single sample analyzed here is the most reduced among all the samples (-4.33 $\Delta \log fO_2$), possibly attesting to the survival of some refractory and diamondiferous mantle domains. However, available data remain too scarce to confidently establish a link between metasomatism and the presence or absence of diamond.

The studied single KL2 eclogitic garnet gives a $\Delta \log fO_2$ (FMQ) value of -0.03 with an uncertainty of ±0.6 log units and lies in the carbonate stability field (Stagno et al. 2015). This value lies at the upper end of the range of $\Delta \log fO_2$ (FMQ) values of KL2 eclogites reported by Shaikh et al. 2023. These are more oxidised in comparison to the peridotitic garnets from the Dharwar cratonic lithosphere and similar to the graphite-diamond-bearing eclogites from Udachnaya kimberlite pipe (Siberian craton) [$\Delta \log fO_2$ (FMQ) -0.01 to -2.4; Mikhailenko et al. 2020]. Although this might reflect the effects of oxidative metasomatism, it is important to note that the eclogite oxybarometer calibrated by Stagno et al. (2015) formally requires the presence of coesite. However, Ca-rich eclogite xenoliths, which are typical for the eclogite component beneath the EDC (Dongre et al. 2015; this study), are often silica-undersaturated, which causes fO_2 to be overestimated (Aulbach et al. 2022). Indeed, the data (this study and published) for eclogitic materials from the Dharwar craton show a positive correlation between CaO and fO_2 (Fig. S7 in the ESM3), and we emphasise that these fO_2 estimates therefore represent a maxima and do not place firm constraints on the stability of carbonate vs. diamond in these samples.

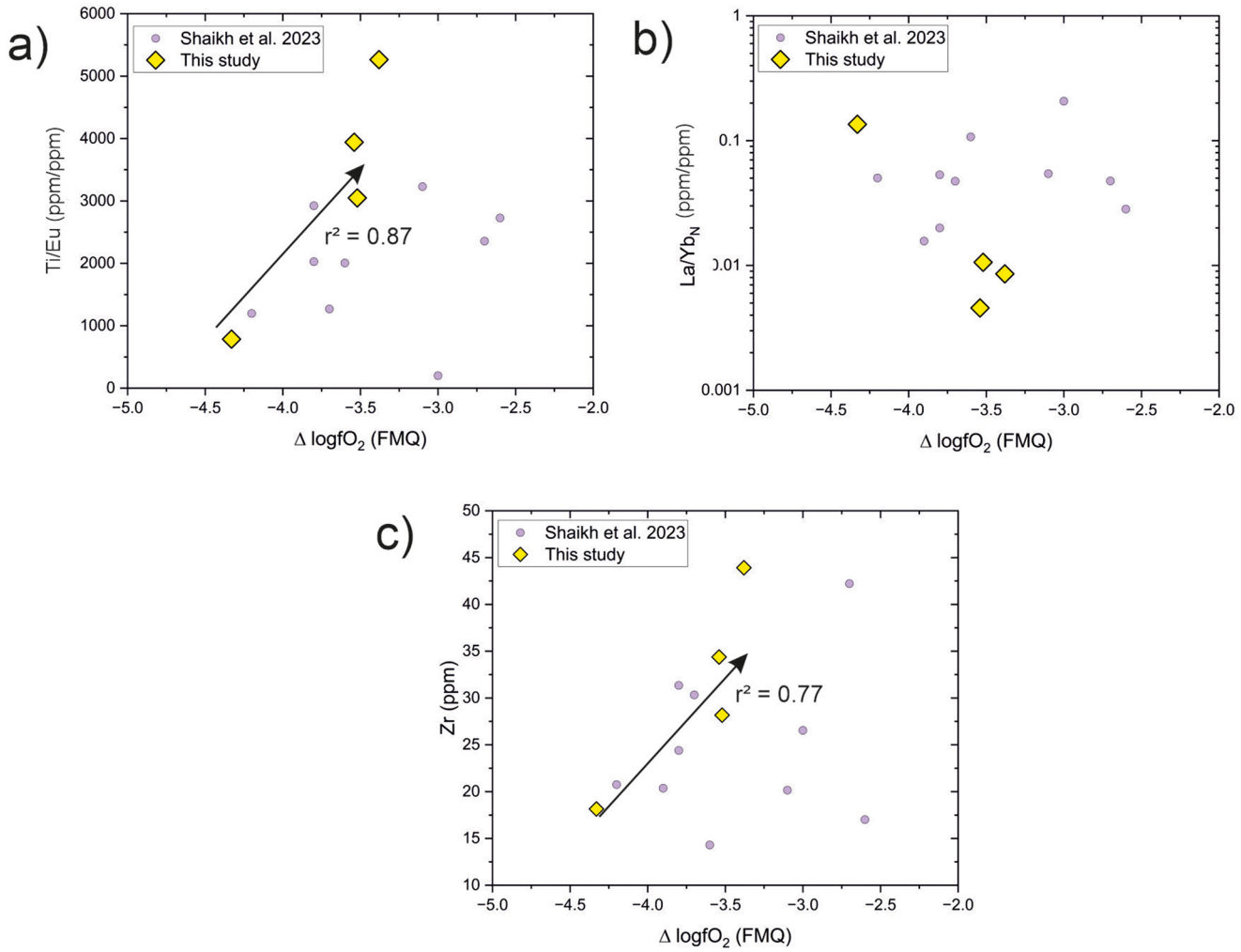


Fig. 9 $\Delta \log fO_2$ (FMQ) plotted against (**a**) Ti/Eu (**b**) La/Yb_N (**c**) Zr for peridotitic garnets and compared with the previous study (Shaikh et al. 2023) from the Eastern Dharwar craton. The positive trends observed in panels (a) and (c) combined with unclear trend of LREE enrichment (panel b) suggest metasomatic oxidation of the sources of these peridotite xenoliths was mediated by kimberlite-like melts

Seismic velocity and mass density of the Dharwar cratonic mantle root: implications for craton evolution

The abundance of eclogite in the cratonic lithosphere varies greatly and estimates range from a few volume percent (2%) based on petrological and heat flow constraints (Schulze 1989; Russell et al. 2001; McLean et al. 2007) to upto 20% based on mass density and gravity signals when compared to dominant peridotite (Garber et al. 2018). Eclogites have calculated mass densities of 3.56 to 3.62 g/cm^3, while peridotites have significantly lower mass densities of 3.29 to 3.32 g/cm^3 and, interestingly, fall at the low end of mass densities estimated for the Siberian peridotites, which equilibrated to an overall colder geotherm (35–38 mW/m^2; Liu et al. 2022) than Dharwar peridotites, illustrating the effect of temperature on mass density (Fig. 10a). The mass-density difference between eclogites and peridotites supports that eclogites play an important role in defining the gravity signals of the cratonic mantle (Garber et al. 2018), and will place upper limits on the volume of this lithology in the regional cratonic lithosphere once gravity data become available.

The structure of the upper mantle beneath the Dharwar craton remains poorly constrained due to insufficient seismic station coverage. However, anomalous bulk lithospheric Vp and Vs, ranging up to 8.9 and 4 km/s, respectively, have been reported in a seismological study by Chaudhury et al. (2021). Seismic velocity estimates from data published in this and prior work (Pattnaik et al. 2020) show that eclogites have calculated Vp and Vs ranges of 8.46 to 8.63 km/s and 4.83 to 4.91 km/s, respectively, which are higher than in peridotites with Vp and Vs ranges of 8.21 to 8.22 km/s and 4.63 to 4.70 km/s (Fig. 10b), but insufficient to explain the observed

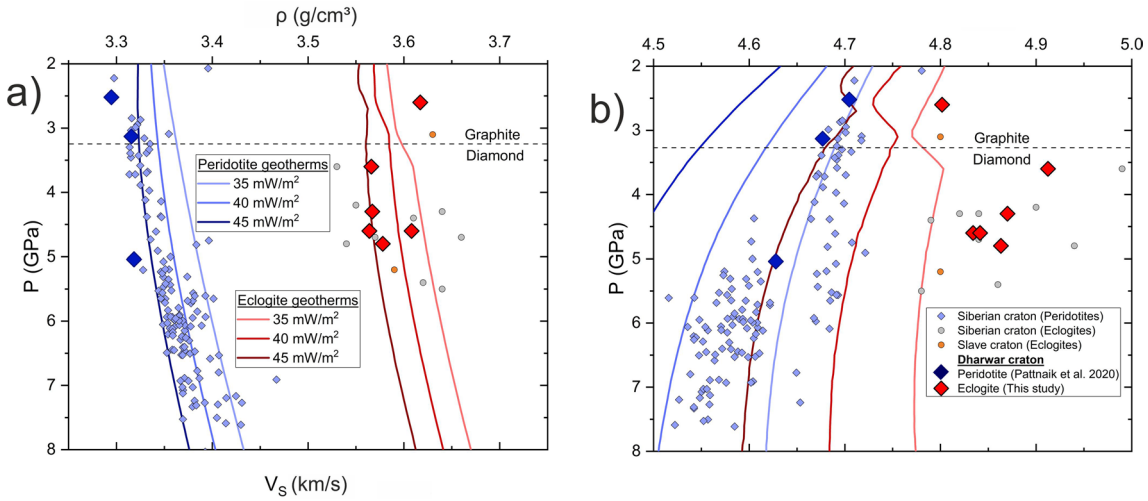


Fig. 10 Physical properties of eclogite (this study) and peridotite (Pattnaik et al. 2020) xenoliths from the Eastern Dharwar craton compared with data for peridotite xenoliths from Siberian craton and eclogite xenoliths from the Slave and Siberian cratons (data sources: this study—Table 1, Pattnaik et al. 2020; Aulbach et al. 2023). The data of the peridotite xenoliths from the Siberian craton are computed from the mineral modes and mineral chemistry from previous studies (Boyd 1984; Sobolev et al. 1984; Boyd et al. 1997; Doucet et al. 2012, 2013; Ionov et al. 2015, 2018, 2020; Goncharov et al. 2012; Agashev et al. 2013; Liu et al. 2022). Variation of (**a**) mass density and (**b**) shear-wave velocity with pressure estimates for eclogite and peridotite xenoliths. Mass density and shear-wave velocity were calculated for eclogite and peridotite xenoliths from the Abers and Hacker (2016) spreadsheet program. The graphite-diamond boundary is after Day (2012). The shear-wave velocities and mass densities of average eclogite and peridotite modeled for geotherms of 35, 40 and 45 mW/m^2 are from Garber et al. (2018)

present-day Vp. A similar discrepancy exists for eclogite xenoliths from the Siberian craton (Aulbach et al. 2023). This, combined with the subordinate volume of eclogite in the cratonic mantle lithosphere, may require that the preferred orientation of olivine contribute to the velocity signal, as suggested for the Siberian craton (Bascou et al. 2011). Alternatively, higher present-day bulk Vp may point to lithological or thermal changes since Mesoproterozoic entrainment, which seems plausible in light of the significant lithosphere thinning documented for the Dharwar craton based on geophysical studies, including heat flow, magnetotelluric, and seismic analyses (Pandey and Agarwal 1999; Kumar et al. 2007a, b).

Conclusions

We report detailed petrography (primary and secondary phases) and major- and trace-element compositions of six eclogite xenoliths (both bimineralic and kyanite-bearing) from the Wajrakarur kimberlites within the EDC, with a particular focus on accessory mineral phases. This study aimed to understand the petrogenesis and post-equilibrium reactions between the eclogite and host kimberlite and the secondary crystallization mineral chemistry of these eclogites. Furthermore, Fe^{3+} measurements were conducted on garnets from peridotite and eclogite xenoliths to gain insight into the oxygen fugacity profile beneath the Dharwar cratonic lithosphere. To further investigate the physical state of the lithospheric mantle beneath the Dharwar craton at the time of kimberlite entrainment, we computed the seismic velocities and mass densities of the peridotite and eclogite xenoliths using geochemical data published in this and prior studies. Therefore, the conclusions of this study highlight several key insights into the origin, evolution, and physicochemical state of the lithospheric mantle beneath the Dharwar craton. These include (i) Positive Sr and Eu anomalies, coupled with increased Al_2O_3 and CaO concentrations and high normative plagioclase modes, indicate a low-pressure, plagioclase-dominant protolith, and their lower SiO_2 and moderate MgO levels suggest minor melt loss during subduction, consistent with previous studies, (ii) The presence of rare grospyditic (high-grossular) garnet and of kyanite associated with clinopyroxene in kyanite eclogites suggests an origin by exsolution due to decompression and lithospheric uplift prior to Mesoproterozoic kimberlite magmatism, (iii) The occurrence of texturally late (post-kelyphite formation) celsian in kyanite eclogites, otherwise devoid of signatures of mantle metasomatism, is consistent with melt infiltration during decompression, implying mantle-kimberlite melt interactions during ascent, (iv) Garnet-$Fe^{3+}/\sum Fe$-based values of $\Delta \log fO_2$ (FMQ) that correlate with indices of melt metasomatism (Zr, Ti) in peridotite xenoliths imply oxidative metasomatic processes, likely driven by carbonated silicate melts, which may have adversely affected diamond grade, and (v) EDC eclogites and peridotites have estimated Vp of 8.46–8.63 km/s and 8.21–8.22 km/s, respectively, which are lower than present-day

observed bulk Vp, and may require lithological or thermal changes since Mesoproterozoic entrainment, possibly related to the previously recognized severe lithosphere thinning ensuing from Gondwana breakup.

Supplementary Information The online version contains supplementary material available at https://doi.org/10.1007/s00710-025-00943-z.

Acknowledgements We are grateful to Ashish Dongre for donating us the mineral separates (KL-2) of eclogite xenoliths from the Eastern Dharwar craton. We gratefully acknowledge Sebastian Peter and Shreya Sarkar from the Mössbauer Spectroscopy facility at the School of Advanced Materials (SAMAT), Jawaharlal Nehru Centre for Advanced Scientific Research (JNCASR), Bangalore, India, for their assistance in analyzing garnet separates for Mössbauer data. We gratefully acknowledge Graham Pearson for his insightful comments and editorial handling of this manuscript, as well as Matthew F. Hardman and an anonymous reviewer for their constructive and valuable feedback. Author JP acknowledges the support for his PhD fellowship from the Ministry of Human Resource Development (MHRD,) Government of India, and a post-doctoral fellowship from the South African National Research Foundation. Author SG acknowledges the support of the ISIRD (start-up grant) from the Indian Institute of Technology Kharagpur and the Science and Engineering Research Board, Department of Science and Technology (SERB–DST), India, via grant ECR/2015/000558. Author SA gratefully acknowledges generous funding by the German Research Foundation (Deutsche Forschungsgemeinschaft), project 467591567. Author FV acknowledges funding from the South African Department of Science and Innovation through their Research Chairs Initiative, as administered by the National Research Foundation (grant 64779). Author RB acknowledges financial support to establish the LA-SF-ICPMS facility at the University of Witwatersrand through an National Research Foundation National Equipment Programme (NRF-NEP) grant (UID 105674). Author EVSSKB thanks Prakash Kumar, Director of the Council for Scientific and Industrial Research National Geophysical Research Institute (CSIR–NGRI), for permission to work on this piece of research and acknowledges support from project MLP-7016-28-EVB.

Funding Open access funding provided by University of Johannesburg.

Open Access This article is licensed under a Creative Commons Attribution 4.0 International License, which permits use, sharing, adaptation, distribution and reproduction in any medium or format, as long as you give appropriate credit to the original author(s) and the source, provide a link to the Creative Commons licence, and indicate if changes were made. The images or other third party material in this article are included in the article's Creative Commons licence, unless indicated otherwise in a credit line to the material. If material is not included in the article's Creative Commons licence and your intended use is not permitted by statutory regulation or exceeds the permitted use, you will need to obtain permission directly from the copyright holder. To view a copy of this licence, visit http://creativecommons.org/licenses/by/4.0/.

References

Abers GA, Hacker BR (2016) A MATLAB toolbox and excel workbook for calculating the densities, seismic wave speeds, and major element composition of minerals and rocks at pressure and temperature. Geochem Geophys Geosyst 17(2):616–624

Agashev AM, Ionov DA, Pokhilenko NP, Golovin AV, Cherepanova Y, Sharygin IS (2013) Metasomatism in lithospheric mantle roots: constraints from whole-rock and mineral chemical composition of deformed peridotite xenoliths from kimberlite pipe Udachnaya. Lithos 160:201–215

Aulbach S (2020) Temperature-dependent rutile solubility in Garnet and clinopyroxene from mantle eclogite: implications for continental crust formation and V-based oxybarometry. J Petrol 61(6):ega–065

Aulbach S, Jacob DE (2016) Major and trace elements in cratonic mantle eclogites and pyroxenites reveal heterogeneous sources and metamorphic processing of low-pressure protoliths. Lithos 262:586–605

Aulbach S, Smart KA (2023) Petrogenesis and geodynamic significance of xenolithic eclogites. Annu Rev Earth Planet Sci 51(1):521–549

Aulbach S, Gerdes A, Viljoen KS (2016) Formation of diamondiferous kyanite–eclogite in a subduction mélange. Geochim Cosmochim Acta 179:156–176

Aulbach S, Woodland AB, Vasilyev P, Gálvez ME, Viljoen KS (2017) Effects of low-pressure igneous processes and subduction on Fe3+/ΣFe and redox state of mantle eclogites from lace (Kaapvaal craton). Earth Planet Sci Lett 474:283–295

Aulbach S, Woodland AB, Stern RA, Vasilyev P, Heaman LM, Viljoen KS (2019) Evidence for a dominantly reducing Archaean ambient mantle from two redox proxies, and low oxygen fugacity of deeply subducted oceanic crust. Sci Rep 9(1):20190

Aulbach S, Massuyeau M, Garber JM, Gerdes A, Heaman LM, Viljoen KS (2020) Ultramafic carbonated Melt-and Auto-Metasomatism in mantle eclogites: compositional effects and geophysical consequences. Geochem Geophys Geosyst 21(5):e2019GC008774

Aulbach S, Woodland AB, Stagno V, Korsakov AV, Mikhailenko D, Golovin A (2022) Fe3 + distribution and Fe3+/ΣFe-oxygen fugacity variations in kimberlite-borne eclogite xenoliths, with comments on clinopyroxene-garnet oxy-thermobarometry. J Petrol 63(8):egac076

Aulbach S, Stalder R, Massuyeau M, Stern RA, Ionov DA, Korsakov AV (2023) Water in Omphacite and Garnet from Pristine Xenolithic Eclogite: T-X-fO2 Controls, Retentivity, and Implications for Electrical Conductivity and Deep H2O Recycling. Geochem Geophys Geosyst 24(12):e2023GC011170

Babu EV, Griffin WL, Panda S, O'Reilly SY, Rao YB (2008) Eclogite xenoliths from the kimberlites of the Eastern Dharwar craton, South india: material representing ancient crust of the Western Dharwar craton?? Int Kimberlite Conf 9

Babu EV, Dash S, Santhosh GH, Mukherjee A (2023) Origin of clinopyroxene megacrysts from the 1.1 Ga Chigicherla-4 kimberlite (CC4), Dharwar craton, Southern india: implications for multistage metasomatism of the sub-continental lithospheric mantle. J Asian Earth Sci 244:105534

Barth MG, Rudnick RL, Horn I, McDonough WF, Spicuzza MJ, Valley JW, Haggerty SE (2001) Geochemistry of xenolithic eclogites from West africa, part I: A link between low MgO eclogites and archean crust formation. Geochim Cosmochim Acta 65(9):1499–1527

Barth MG, Rudnick RL, Horn I, McDonough WF, Spicuzza MJ, Valley JW, Haggerty SE (2002) Geochemistry of xenolithic eclogites from West africa, part 2: origins of the high MgO eclogites. Geochim Cosmochim Acta 66(24):4325–4345

Bascou J, Doucet LS, Saumet S, Ionov DA, Ashchepkov IV, Golovin AV (2011) Seismic velocities, anisotropy and deformation in Siberian cratonic mantle: EBSD data on xenoliths from the Udachnaya kimberlite. Earth Planet Sci Lett 304(1–2):71–84

Benoit M, Polvé M, Ceuleneer G (1996) Trace element and isotopic characterization of mafic cumulates in a fossil mantle diapir (Oman ophiolite). Chem Geol 134(1–3):199–214
Beyer C, Frost DJ, Miyajima N (2015) Experimental calibration of a garnet–clinopyroxene geobarometer for mantle eclogites. Contrib Mineral Petrol 169(2):18
Bidyananda M, Deomurari MP, Goswami JN (2003) 207 Pb–206 Pb ages of zircons from the nuggihalli schist belt, Dharwar craton, Southern India. Curr Sci 1482–1485
Boyd FR (1984) Siberian geotherm based on iherzolite xenoliths from the Udachnaya kimberlite, USSR. Geology 12(9):528–530
Boyd FR, Pokhilenko NP, Pearson DG, Mertzman SA, Sobolev NV, Finger LW (1997) Composition of the Siberian cratonic mantle: evidence from Udachnaya peridotite xenoliths. Contrib Mineral Petrol 128(2):228–246
Burness S, Smart KA, Tappe S, Stevens G, Woodland AB, Cano E (2020) Sulphur-rich mantle metasomatism of Kaapvaal craton eclogites and its role in redox-controlled platinum group element mobility. Geochem Geophys Geosyst 542:119476
Caporuscio FA, Smyth JR (1987) Variable LREE enrichment of mantle eclogites from South Africa by MARID fluids (abstracts program). Geol Soc Am 19:250
Caporuscio FA, Smyth JR (1990) Trace element crystal chemistry of mantle eclogites. Contrib Mineral Petrol 105(5):550–561
Carswell DA, Dawson JB, Gibb FGF (1981) Equilibration conditions of upper-mantle eclogites: implications for kyanite-bearing and diamondiferous varieties. Mineral Mag 44(333):79–89
Chadwick B, Vasudev VN, Hegde GV (2000) The Dharwar craton, Southern india, interpreted as the result of late Archaean oblique convergence. Precambrian Res 99(1–2):91–111
Chalapathi Rao NC, Miller JA, Pyle DM, Madhavan V (1996) New proterozoic K-Ar ages for some kimberlites and lamproites from the Cuddapah basin and Dharwar craton, South india: evidence for non-contemporaneous emplacement. Precambrian Res 79(3–4):363–369
Chalapathi Rao NV, Wu FY, Mitchell RH, Li QL, Lehmann B (2013) Mesoproterozoic U–Pb ages, trace element and Sr–Nd isotopic composition of perovskite from kimberlites of the Eastern Dharwar craton, Southern india: distinct mantle sources and a widespread 1.1 Ga tectonomagmatic event. Chem Geol 353:48–64
Chatterjee A, Rao NC, Pandey R, Pandey A (2023) Mantle transition zone-derived eclogite xenolith entrained in a diamondiferous mesoproterozoic (∼1.1 Ga) kimberlite from the Eastern Dharwar craton, india: evidence from a coesite, K-omphacite, and majoritic Garnet assemblage. Geol Mag 160(5):874–887
Chaudhury J, Mitra S, Sarkar T (2021) Hales discontinuity in the Southern Indian continental lithosphere: seismological and petrological models. J Geophys Res Solid Earth 126(2):e2020JB020564
Chinner GA, Cornell DH (1974) Evidence of kimberlite-grospydite reaction. Contrib Mineral Petrol 45(2):153–160
Coleman RG, Lee DE, Beatty LB, Brannock WW (1965) Eclogites and eclogites: their differences and similarities. Geol Soc Am Bull 76(5):483–508
Creighton S, Stachel T, Matveev S, Höfer H, McCammon C, Luth RW (2009) Oxidation of the Kaapvaal lithospheric mantle driven by metasomatism. Contrib Mineral Petrol 157:491–504
Creighton S, Stachel T, Eichenberg D, Luth RW (2010) Oxidation state of the lithospheric mantle beneath Diavik diamond mine, central slave craton, NWT, Canada. Contrib Mineral Petrol 159:645–657
Dawson JB, Harley SL (2009) Some post-equilibrium reactions in kimberlite-derived eclogites paper A-00081. Lithos 112:1025–1031
Day HW (2012) A revised diamond-graphite transition curve. Am Mineral 97(1):52–62
Dongre AN, Jacob DE, Stern RA (2015) Subduction-related origin of eclogite xenoliths from the Wajrakarur kimberlite field, Eastern Dharwar craton, Southern india: constraints from petrology and geochemistry. Geochim Cosmochim Acta 166:165–188
Dongre A, Rao NC, Viljoen KS, Lehmann B (2017) Petrology, genesis and geodynamic implication of the Mesoproterozoic–Late cretaceous Timmasamudram kimberlite cluster, Wajrakarur field, Eastern Dharwar craton, Southern India. Geosci Front 8(3):541–553
Doucet LS, Ionov DA, Golovin AV, Pokhilenko NP (2012) Depth, degrees and tectonic settings of mantle melting during craton formation: inferences from major and trace element compositions of spinel Harzburgite xenoliths from the Udachnaya kimberlite, central Siberia. Earth Planet Sci Lett 359:206–218
Doucet LS, Ionov DA, Golovin AV (2013) The origin of coarse Garnet peridotites in cratonic lithosphere: new data on xenoliths from the Udachnaya kimberlite, central Siberia. Contrib Mineral Petrol 165:1225–1242
Friend CRL, Nutman AP (1991) SHRIMP U-Pb geochronology of the closepet granite and Peninsular gneiss, karnataka, South India. J Geol Soc India 38(4):357–368
Gale A, Dalton CA, Langmuir CH, Su Y, Schilling JG (2013) The mean composition of ocean ridge basalts. Geochem Geophys Geosyst 14(3):489–518
Ganguly J, Bhattacharya PK (1987) Xenoliths in proterozoic kimberlites from Southern india: petrology and geophysical implications. In: Mantle xenoliths, Wiley-Interscience, pp 249–265
Garber JM, Maurya S, Hernandez JA, Duncan MS, Zeng L, Zhang HL, Faul U, McCammon C, Montagner JP, Moresi L, Romanowicz BA (2018) Multidisciplinary constraints on the abundance of diamond and eclogite in the cratonic lithosphere. Geochem Geophys Geosyst 19(7):2062–2086
Godard M, Awaji S, Hansen H, Hellebrand E, Brunelli D, Johnson K, Yamasaki T, Maeda J, Abratis M, Christie D, Kato Y (2009) Geochemistry of a long in-situ Stion of intrusive slow-spread oceanic lithosphere: results from IODP site U1309 (Atlantis massif, 30 N Mid-Atlantic-Ridge). Earth Planet Sci Lett 279(1–2):110–122
Goncharov AG, Ionov DA (2012) Redox state of deep off-craton lithospheric mantle: new data from Garnet and spinel peridotites from vitim, Southern Siberia. Contrib Mineral Petrol 164:731–745
Gopalan K, Kumar A (2008) Phlogopite K–Ca dating of Narayanpet kimberlites, South india: implications to the discordance between their Rb–Sr and ar/ar ages. Precambrian Res 167(3–4):377–382
Griffin WL, Kobussen AF, Babu EVSSK, O'Reilly SY, Norris R, Sengupta P (2009) A translithospheric suture in the vanished 1-Ga lithospheric root of South india: evidence from contrasting lithosphere stions in the Dharwar craton. Lithos 112:1109–1119
Hanger BJ, Yaxley GM, Berry AJ, Kamenetsky VS (2015) Relationships between oxygen fugacity and metasomatism in the Kaapvaal subcratonic mantle, represented by Garnet peridotite xenoliths in the Wesselton kimberlite, South Africa. Lithos 212:443–452
Harley SL, Carswell DA (1995) Ultradeep crustal metamorphism: A prospective view. J Geophys Res Solid Earth 100(B5):8367–8380
Harte B, Kirkley MB (1997) Partitioning of trace elements between clinopyroxene and garnet: data from mantle eclogites. Chem Geol 136(1–2):1–24
Hasterok D, Chapman DS (2011) Heat production and geotherms for the continental lithosphere. Earth Planet Sci Lett 307(1–2):59–70
Heaman LM, Creaser RA, Cookenboo HO (2002) Extreme enrichment of high field strength elements in Jericho eclogite xenoliths: A cryptic record of paleoproterozoic subduction, partial melting, and metasomatism beneath the slave craton, Canada. Geology 30(6):507–510
Heaman LM, Creaser RA, Cookenboo HO, Chacko TOM (2006) Multi-stage modification of the Northern slave mantle lithosphere: evidence from zircon-and diamond-bearing eclogite xenoliths entrained in Jericho kimberlite, Canada. J Petrol 47(4):821–858

Hills DV, Haggerty SE (1989) Petrochemistry of eclogites from the Koidu kimberlite complex, Sierra Leone. Contrib Mineral Petrol 103(4):397–422

Höfer HE, Brey GP (2007) The iron oxidation state of Garnet by electron microprobe: its determination with the flank method combined with major-element analysis. Am Mineral 92(5–6):873–885

Ionov DA, Doucet LS, Carlson RW, Golovin AV, Korsakov AV (2015) Post-Archean formation of the lithospheric mantle in the central Siberian craton: Re–Os and PGE study of peridotite xenoliths from the Udachnaya kimberlite. Geochim Cosmochim Acta 165:466–483

Ionov DA, Doucet LS, Xu Y, Golovin AV, Oleinikov OB (2018) Reworking of archean mantle in the NE Siberian craton by carbonatite and silicate melt metasomatism: evidence from a carbonate-bearing, dunite-to-websterite xenolith suite from the Obnazhennaya kimberlite. Geochim Cosmochim Acta 224:132–153

Ionov DA, Liu Z, Li J, Golovin AV, Korsakov AV, Xu Y (2020) The age and origin of cratonic lithospheric mantle: archean Dunites vs. Paleoproterozoic Harzburgites from the Udachnaya kimberlite, Siberian craton. Geochim Cosmochim Acta 281:67–90

Ireland TR, Rudnick RL, Spetsius Z (1994) Trace elements in diamond inclusions from eclogites reveal link to archean granites. Earth Planet Sci Lett 128(3–4):199–213

Ishikawa A, Pearson G, Maruyama S, de Bruin D, Gurney J (2008) Compositional variability of the Roberts victor eclogites: evidence for mantle metasomatism involving diamond dissolution. Int Kimberl Conf: Ext Abstr 9. https://doi.org/10.29173/ikc3328

Jacob DE (2004) Nature and origin of eclogite xenoliths from kimberlites. Lithos 77(1–4):295–316

Jacob DE, Foley SF (1999) Evidence for archean ocean crust with low high field strength element signature from diamondiferous eclogite xenoliths. Lithos 48(1–4):317–336

Jacob D, Jagoutz E, Lowry D, Mattey D, Kudrjavtseva G (1994) Diamondiferous eclogites from siberia: remnants of archean oceanic crust. Geochim Cosmochim Acta 58(23):5191–5207

Jacob DE, Schmickler B, Schulze DJ (2003) Trace element geochemistry of coesite-bearing eclogites from the Roberts victor kimberlite, Kaapvaal craton. Lithos 71(2–4):337–351

Jacob DE, Viljoen KS, Grassineau NV (2009) Eclogite xenoliths from kimberley, South Africa—a case study of mantle metasomatism in eclogites. Lithos 112:1002–1013

Jayananda M, Moyen JF, Martin H, Peucat JJ, Auvray B, Mahabaleswar B (2000) Late Archaean (2550–2520 Ma) juvenile magmatism in the Eastern Dharwar craton, Southern india: constraints from geochronology, Nd–Sr isotopes and whole rock geochemistry. Precambrian Res 99(3–4):225–254

Jenner FE, O'Neill HSC (2012) Analysis of 60 elements in 616 ocean floor basaltic glasses. Geochem Geophys Geosyst 13

Jerde EA, Taylor LA, Crozaz G, Sobolev NV, Sobolev VN (1993) Diamondiferous eclogites from yakutia, siberia: evidence for a diversity of protoliths. Contrib Mineral Petrol 114(2):189–202

Jochum KP, Nohl U, Herwig K, Lammel E, Stoll B, Hofmann AW (2005) GeoReM: a new geochemical database for reference materials and isotopic standards. Geostand Geoanal Res 29(3):333–338

Jochum KP, Weis U, Stoll B, Kuzmin D, Yang Q, Raczek I, Jacob DE, Stracke A, Birbaum K, Frick DA, Günther D (2011) Determination of reference values for NIST SRM 610–617 glasses following ISO guidelines. Geostand Geoanal Res 35(4):397–429

Johannsen A (1937) A descriptive petrography of the igneous rocks. Geol Assoc Stockholm Negot 59(3):363–364

Karmalkar NR, Duraiswami RA, Chalapathi Rao NV, Paul DK (2009) Mantle-derived mafic-ultramafic xenoliths and the nature of Indian sub-continental lithosphere. J Geol Soc India 73(5):657

Korolev N, Nikitina LP, Goncharov A, Dubinina EO, Melnik A, Müller D, Chen YX, Zinchenko VN (2021) Three types of mantle eclogite from two layers of oceanic crust: a key case of metasomatically aided transformation of low-to-high-magnesian eclogite. J Petrol 62(11):egab070

Krogh EJ (1988) The garnet-clinopyroxene Fe-Mg geothermometer—a reinterpretation of existing experimental data. Contrib Mineral Petrol 99(1):44–48

Kukkonen IT, Kinnunen KA, Peltonen P (2003) Mantle xenoliths and Thick lithosphere in the Fennoscandian shield. Phys Chem Earth 28(9–11):349–360

Kumar A, Heaman LM, Manikyamba C (2007a) Mesoproterozoic kimberlites in South india: A possible link to∼ 1.1 Ga global magmatism. Precambrian Res 154(3–4):192–204

Kumar P, Yuan X, Kumar MR, Kind R, Li X, Chadha RK (2007b) The rapid drift of the Indian tectonic plate. Nature 449(7164):894–897

Lappin MA (1978) The evolution of a grospydite from the Roberts victor mine, South Africa. Contrib Mineral Petrol 66:229–241

Lappin MA, Dawson JB (1975) Two Roberts victor cumulate eclogites and their re–equilibration. In: Physics and Chemistry of the Earth Pergamon, pp 351–365

Lazarov M, Woodland AB, Brey GP (2009) Thermal state and redox conditions of the Kaapvaal mantle: A study of xenoliths from the Finsch mine, South Africa. Lithos 112:913–923

Litasov KD, Shatskiy A, Ohtani E (2014) Melting and subsolidus phase relations in peridotite and eclogite systems with reduced COH fluid at 3–16 GPa. Earth Planet Sci Lett 391:87–99

Liu Z, Ionov DA, Nimis P, Xu Y, He P, Golovin AV (2022) Thermal and compositional anomalies in a detailed xenolith-based lithospheric mantle profile of the Siberian craton and the origin of seismic midlithosphere discontinuities. Geology 50(8):891–896

MacGregor ID, Manton WI (1986) Roberts victor eclogites: ancient oceanic crust. J Geophys Res Solid Earth 91(B14):14063–14079

Marras G, Mikhailenko D, McCammon CA, Logvinova A, Hanžel D, Dallai L, Stagno V (2025) Oxy-thermobarometry of grospydite and high-Ca eclogite xenoliths from Zagadochnaya kimberlite pipe (Yakutia, Siberian craton). Mineral Petrol 1–19

McCammon C, Kopylova MG (2004) A redox profile of the slave mantle and oxygen fugacity control in the cratonic mantle. Contrib Mineral Petrol 148:55–68

McCormick TC, Smyth JR, Caporuscio FA (1994) Chemical systematics of sondary phases in mantle eclogites. Kimberlites Relat Rocks Mantle Xenoliths 1:405–419

McDonough WF, Sun SS (1995) The composition of the Earth. Chem Geol 120(3–4):223–253

McLean H, Banas A, Creighton S, Whiteford S, Luth RW, Stachel T (2007) Garnet xenocrysts from the Diavik mine, NWT, canada: composition, color, and paragenesis. Can Mineral 45(5):1131–1145

Mikhailenko DS, Stagno V, Korsakov AV, Andreozzi GB, Marras G, Cerantola V, Malygina EV (2020) Redox state determination of eclogite xenoliths from Udachnaya kimberlite pipe (Siberian craton), with some implications for the graphite/diamond formation. Contrib Mineral Petrol 175:1–17

Mikhailenko DS, Aulbach S, Korsakov AV, Golovin AV, Malygina EV, Gerdes A, Stepanov AS, Xu YG (2021) Origin of graphite–diamond-bearing eclogites from Udachnaya kimberlite pipe. J Petrol 62(8):egab033

Mikhailenko DS, Aulbach S, Stepanov AS, Korsakov AV, Zhang L, Xu YG (2024) Allanite in mantle eclogite xenoliths. J Petrol 65(5):egae041

Misra KC, Anand M, Paul DK (2008) Metasomatized Kyanite-eclogites xenoliths from a Southern Indian kimberlite, 9Ext Abstr, edn. Int Kimberlite Conf

Morimoto N (1989) Nomenclature of pyroxenes. Min Petrol 39(1):55–76

Naqvi SM, Rogers JJW (1987) Precambrian geology of india. Oxford monographs on geology and geophysics. Oxford University Press Oxford, p 223

Nayak SS, Kudari SAD (1999) Discovery of diamond-bearing kimberlites in Kalyandurg area, Anantapur district, Andhra Pradesh. Curr Sci 76(8):1077–1079

Neelakantam S (2001) Exploration for diamonds in Southern India. Geol Surv India Spec Pub 58:521–555

Nehru CE, Reddy AK (1989) Ultramafic xenoliths from Vajrakarur kimberlites, India. Geol Soc Aust Spec Publ 14:745–758

Nikitina LP, Korolev NM, Zinchenko VN, Felix JT (2014) Eclogites from the upper mantle beneath the Kasai craton (Western Africa): Petrography, whole-rock geochemistry and U-Pb zircon age. Precambrian Res 249:13–32

O'Neill HSC, Wall VJ (1987) The Olivine—Orthopyroxene—Spinel oxygen geobarometer, the nickel precipitation curve, and the oxygen fugacity of the earth's upper mantle. J Petrol 28(6):1169–1191

O'Reilly SY, Griffin WL (1995) Trace-element partitioning between garnet and clinopyroxene in mantle-derived pyroxenites and eclogites: PTX controls. Chem Geol 121(1-4):105–130

Ongley JS, Basu AR, Kyser TK (1987) Oxygen isotopes in coexisting garnets, clinopyroxenes and phlogopites of Roberts victor eclogites: implications for petrogenesis and mantle metasomatism. Earth Planet Sci Lett 83(1–4):80–84

Osborne I, Sherlock S, Anand M, Argles T (2011) New Ar–Ar ages of Southern Indian kimberlites and a lamproite and their geochemical evolution. Precamb Res 189(1–2):91–103

Pandey OP, Agrawal PK (1999) Lithospheric mantle deformation beneath the Indian cratons. J Geol 107(6):683–692

Patel SC, Ravi S, Thakur SS, Rao TK, Subbarao KV (2006) Eclogite xenoliths from Wajrakarur kimberlites, Southern India. Mineral Pet 88(1–2):363

Patel SC, Ravi S, Anilkumar Y, Naik A, Thakur SS, Pati JK, Nayak SS (2009) Mafic xenoliths in proterozoic kimberlites from Eastern Dharwar craton, india: mineralogy and P–T regime. J Asian Earth Sci 34(3):336–346

Paton C, Woodhead JD, Hellstrom JC, Hergt JM, Greig A, Maas R (2010) Improved laser ablation U-Pb Zircon geochronology through robust downhole fractionation correction. Geochem Geophys Geosyst 11(3)

Paton C, Hellstrom J, Paul B, Woodhead J, Hergt J (2011) Iolite: freeware for the visualisation and processing of mass spectrometric data. J Anal Spectrom 26(12):2508–2518

Pattnaik J, Aulbach S, Viljoen F, Ueckermann H, Mxinwa T (2025) The diamond-poor nature of corundum-bearing eclogite and Karoo-type overprint of deep eclogite sources beneath the Kimberley region (Kaapvaal craton). J Petrol 66(3):egaf011

Pattnaik J, Ghosh S, Dongre A (2020) Plume activity and carbonated silicate melt metasomatism in Dharwar cratonic lithosphere: evidence from peridotite xenoliths in Wajrakarur kimberlites. Lithos 376:105726

Pattnaik J, Demouchy S, Ghosh S (2021) Low hydrogen concentrations in Dharwar cratonic lithosphere inferred from peridotites, Wajrakarur kimberlites field: implications for mantle viscosity and carbonated silicate melt metasomatism. Precamb Res 352:105982

Peltonen P, Kinnunen KA, Huhma H (2002) Petrology of two diamondiferous eclogite xenoliths from the Lahtojoki kimberlite pipe, Eastern Finland. Lithos 63(3–4):151–164

Pyle JM, Haggerty SE (1994) Silicate-carbonate liquid immiscibility in upper-mantle eclogites: implications for Natrosilicic and carbonatitic conjugate melts. Geochim Cosmochim Acta 58(14):2997–3011

Radu IB, Moine BN, Bolfan-Casanova N, Ionov DA, Devidal JL, Deloule, Cottin JY (2022) Zoisite in cratonic eclogite xenoliths-Implications for water in the upper mantle. Lithos 418:106681

Ramakrishnan M, Vaidyanadhan R (2010) Geology of India (1 & 2). GSI Publ 2(1)

Ravi S, Sufija MV, Patel SC, Sheikh JM, Sridhar M, Kaminsky FV, Rao KB (2013) Diamond potential of the Eastern Dharwar Craton, southern India, and a reconnaissance study of physical and infrared characteristics of the diamonds. In: Proc 10th Int Kimberlite Conf, Springer, pp 335–48

Rudnick RL (1995) Making continental crust. Nature 378(6557):571–578

Russell JK, Dipple GM, Kopylova MG (2001) Heat production and heat flow in the mantle lithosphere, slave craton, Canada. Phys Earth Planet Inter 123(1):27–44

Satyanarayana SV (2002) Diamond Provinces of India: an overview. In Proceedings of the International Conference on Diamond & Gemstones organized by South Asian Association of Economic Geologists (SAAEG) at Raipur, Chattisgarh, India. pp 9–15

Schmickler B, Jacob DE, Foley SF (2004) Eclogite xenoliths from the Kuruman kimberlites, South africa: geochemical fingerprinting of deep subduction and cumulate processes. Lithos 75(1–2):173–207

Schmidt M, Poli S (2013) Devolatilization during subduction. Treatise Geochem 4:669–701

Schulze DJ (1989) Constraints on the abundance of eclogite in the upper mantle. J Geophys Res Solid Earth 94(B4):4205–4212

Schulze DJ, Helmstaedt H (1988) Coesite-sanidine eclogites from kimberlite: products of mantle fractionation or subduction? J Geol 96(4):435–443

Shaikh AM, Bussweiler Y, Viljoen F, Bolhar R, Ravi S, Hezel DC, Ueckermann H, Tappe S (2023) Redox state of the Dharwar craton root as inferred from eclogite and peridotite sourced mantle cargo, with implications for kimberlite and lamproite magma formation. Contrib Min Pet 178(12):86

Shchukina EV, Agashev AM, Zedgenizov DA (2018) Origin of zircon-bearing mantle eclogites entrained in the V. Grib kimberlite (Arkhangelsk region, NW Russia): Evidence from mineral geochemistry and the U-Pb and Lu-Hf isotope compositions of zircon. Min Pet 112:85–100

Shu Q, Brey GP, Hoefer HE, Zhao Z, Pearson DG (2016) Kyanite/corundum eclogites from the Kaapvaal craton: subducted troctolites and layered Gabbros from the Mid-to early archean. Contrib Min Pet 171(2):11

Smart KA, Chacko T, Simonetti A, Sharp ZD, Heaman LM (2014) A record of paleoproterozoic subduction preserved in the Northern slave cratonic mantle: Sr-Pb-O isotope and trace-element investigations of eclogite xenoliths from the Jericho and muskox kimberlites. J Pet 55(3):549–583

Smart KA, Tappe S, Simonetti A, Simonetti SS, Woodland AB, Harris C (2017) Tectonic significance and redox state of paleoproterozoic eclogite and pyroxenite components in the slave cratonic mantle lithosphere, Voyageur kimberlite, Arctic Canada. Chem Geol 455:98–119

Smart KA, Tappe S, Woodland AB, Harris C, Corcoran L, Simonetti A (2021) Metasomatized eclogite xenoliths from the central Kaapvaal craton as probes of a seismic mid-lithospheric discontinuity. Chem Geol 578:120286

Smith CB, Haggerty SE, Chatterjee B, Beard A, Townend R (2013) Kimberlite, lamproite, ultramafic lamprophyre, and carbonatite relationships on the Dharwar craton, india; an example from the Khaderpet pipe, a diamondiferous ultramafic with associated carbonatite intrusion. Lithos 182:102–113

Smyth JR (1980) Cation vacancies and the crystal chemistry of breakdown reactions in kimberlitic omphacites. Am Min 65(11–12):1185–1191

Smyth JR, Caporuscio FA (1984) Petrology of a suite of eclogite inclusions from the Bobbejaan kimberlite: II. Primary phase compositions and origin. Developments Petrol 11:121–131

Smyth JR, Caporuscio FA, McCormick TC (1989) Mantle eclogites: evidence of igneous fractionation in the mantle. Earth Planet Sci Lett 93(1):133–141

Sobolev NV Jr (1968) Eclogite clinopyroxenes from the kimberlite pipes of Yakutia. Lithos 1(1):54–57

Sobolev NV, Pokhilenko NP, Lavrent'ev YG, Yefimova ES (1977) Deep-seated xenoliths, xenocrysts in kimberlites and crystalline inclusions in diamonds from Udachnaya kimberlite pipe, Yakutia. Int Kimberl Conf Ext Abstr 2:328–330

Sobolev NV, Pokhilenko NP, Efimova ES (1984) Diamond-bearing peridotite xenoliths in kimberlites and the problem of the origin of diamonds. Geol Geofiz 25(12):62–76

Sommer H, Jacob DE, Stern RA, Petts D, Mattey DP, Pearson DG (2017) Fluid-induced transition from banded kyanite-to bimineralic eclogite and implications for the evolution of cratons. Geochim Cosmochim Acta 207:19–42

Stagno V, Ojwang DO, McCammon CA, Frost DJ (2013) The oxidation state of the mantle and the extraction of carbon from earth's interior. Nature 493(7430):84–88

Stagno V, Frost DJ, McCammon CA, Mohseni H, Fei Y (2015) The oxygen fugacity at which graphite or diamond forms from carbonate-bearing melts in eclogitic rocks. Contrib Min Pet 169:1–18

Sudholz ZJ, Yaxley GM, Jaques AL, Chen J (2021) Ni-in-garnet geothermometry in mantle rocks: a high-pressure experimental recalibration between 1100 and 1325°C. Contrib Min Pet 176:1–16

Sun SS, McDonough WF (1989) Chemical and isotopic systematics of oceanic basalts: implications for mantle composition and processes. Geol Soc Lond Spec Pub 42(1):313–345

Tappe S, Smart KA, Pearson DG, Steenfelt A, Simonetti A (2011) Craton formation in late archean subduction zones revealed by first Greenland eclogites. Geology 39(12):1103–1106

Taylor LA, Neal CR (1989) Eclogites with oceanic crustal and mantle signatures from the Bellsbank kimberlite, South africa, part I: mineralogy, petrography, and whole rock chemistry. J Geol 97(5):551–567

Veeraswamy K, Raval U (2005) Remobilization of the palaeoconvergent corridors hidden under the Deccan trap cover and some major stable continental region earthquakes. Curr Sci 10:522–530

Williams HM, Nielsen SG, Renac C, Griffin WL, O'Reilly SY, McCammon CA, Pearson N, Viljoen F, Alt JC, Halliday AN (2009) Fractionation of oxygen and iron isotopes by partial melting processes: implications for the interpretation of stable isotope signatures in mafic rocks. Earth Planet Sci Lett 283(1–4):156–166

Woodland AB, Koch M (2003) Variation in oxygen fugacity with depth in the upper mantle beneath the Kaapvaal craton, Southern Africa. Earth Planet Sci Lett 214(1–2):295–310

Woodland AB, Peltonen P (1998) Ferric/ferrous iron contents of Garnet and clinopyroxene and calculated oxygen fugacities of peridotite xenoliths from the Eastern Finland kimberlite Province. Int Kimberl Conf Ext Abstr 7:963–964

Woodland AB, Gräf C, Sandner T, Höfer HE, Seitz HM, Pearson DG, Kjarsgaard BA (2021) Oxidation state and metasomatism of the lithospheric mantle beneath the rae craton, canada: strong gradients reflect craton formation and evolution. Sci Rep 11(1):3684

Yaxley GM, Berry AJ, Kamenetsky VS, Woodland AB, Golovin AV (2012) An oxygen fugacity profile through the Siberian Craton—Fe K-edge XANES determinations of Fe3+/∑Fe in garnets in peridotite xenoliths from the Udachnaya East kimberlite. Lithos 140:142–151

Yaxley GM, Berry AJ, Rosenthal A, Woodland AB, Paterson D (2017) Redox preconditioning deep cratonic lithosphere for kimberlite genesis–evidence from the central slave craton. Sci Rep 7(1):30

Publisher's note Springer Nature remains neutral with regard to jurisdictional claims in published maps and institutional affiliations.